

Article

# Quantitative Phase Analysis of Skarn Rocks by the Rietveld Method Using X-ray Powder Diffraction Data

Yana Tzvetanova <sup>1</sup>, Ognyan Petrov <sup>1</sup>, Thomas Kerestedjian <sup>2,\*</sup> and Mihail Tarassov <sup>1</sup>

<sup>1</sup> Institute of Mineralogy and Crystallography, Bulgarian Academy of Sciences, 1113 Sofia, Bulgaria; yana.tzvet@gmail.com (Y.T.); opetrov@dir.bg (O.P.); mptarass@dir.bg (M.T.)

<sup>2</sup> Geological Institute, Bulgarian Academy of Sciences, Acad. G. Bonchev Str., 24 Bl., 1113 Sofia, Bulgaria

\* Correspondence: thomas@geology.bas.bg

Received: 9 September 2020; Accepted: 7 October 2020; Published: 9 October 2020



**Abstract:** The Rietveld method using X-ray powder diffraction data was applied to selected skarn samples for quantitative determination of the present minerals. The specimens include garnet, clinopyroxene–garnet, plagioclase–clinopyroxene–wollastonite–garnet, plagioclase–clinopyroxene–wollastonite, plagioclase–clinopyroxene–wollastonite–epidote, and plagioclase–clinopyroxene skarns. The rocks are coarse- to fine-grained and characterized by an uneven distribution of the constituent minerals. The traditional methods for quantitative analysis (point-counting and norm calculations) are not applicable for such inhomogeneous samples containing minerals with highly variable chemical compositions. Up to eight individual mineral phases have been measured in each sample. To obtain the mineral quantities in the skarn rocks preliminary optical microscopy and chemical investigation by electron probe microanalysis (EPMA) were performed for the identification of some starting components for the Rietveld analysis and to make comparison with the Rietveld X-ray powder diffraction results. All of the refinements are acceptable, as can be judged by the standard indices of agreement and by the visual fits of the observed and calculated diffraction profiles. A good correlation between the refined mineral compositions and the data of the EPMA measurements was achieved.

**Keywords:** quantitative phase analysis; skarn minerals; Rietveld method

## 1. Introduction

The estimation of relative quantities of the constituent minerals in rocks is essential for their classification and determination of paragenesis as well as for studies of their genesis, sequence of different mineralogical stages and geological events. The mineral modal analysis is also important for assessment of potentially valuable minerals and is applied in multi-component systems such as cements, ceramics, and archaeological materials.

The Rietveld method is one of the most appropriate techniques for modal analysis of rocks and synthetic polycrystalline materials based on X-ray powder diffraction (XRPD). This method was originally developed for the refinement of structures studied with neutron-diffraction [1,2] and subsequently was successfully applied to crystal-structure refinements of minerals and synthetic equivalents investigated with X-ray powder diffraction and synchrotron radiation [3–6]. This methodology and the possibilities for quantitative analysis were developed in detail in the works of: Albinati and Willis [7], Hill [8], Hill and Madsen [9], Hill and Howard [10], Bish and Howard [11], Post and Bish [12], Snyder and Bish [13], Hill [14], Young [15].

The Rietveld XRPD method is a full-profile approach for quantitative analysis based on a least squares fit between the calculated diffraction pattern and the observed experimental data of a measured

diffraction pattern. In this technique, the simulated XRPD pattern is calculated from the structural parameters of each mineral (atomic coordinates, site occupancies, unit cell parameters, etc.), the scale factor for each constituent phase, experimental parameters affecting the pattern, effects resulting from preferred orientation, crystallite size and degree of microstrain, parameters describing the peak profile and the background. The phase abundances are directly calculated from the refined scale-factors.

The quantitative mineralogical analysis using Rietveld XRPD method has significant advantages over other traditional methods such as (i) point-counting or image analyses of thin sections, (ii) conventional X-ray powder-diffraction measurements using integrated peak-intensities, and (iii) normative calculations based on whole-rock chemical composition [16]. One of the main advantages is that during the analytical procedure the crystal chemistry and physical properties of each of the phases can be adjusted. The possibility to refine the unit cell parameters, occupancy and site coordinates allows extracting additional information from the powder diffraction pattern [17]. A detailed review of the advantages and disadvantages of each of the above methods was made by Hill et al. [18].

Systematic results on the application of Rietveld XRPD quantitative analysis to geological samples have been reported by Hill et al. [18] for determination of mineral abundances in a range of igneous, volcanic, and metamorphic rocks, by Mumme et al. [19] in sedimentary rocks, and by Mumme et al. [20] in massive sulfide ores. The method was successfully applied to various geological materials—montmorillonite rocks [21]; wollastonite skarns [22]; hydrothermally altered rocks [23]; heavy minerals in sandstones [24]; dacitic rocks [25]; pyrite and other sulfide minerals in mine rock piles [26]; bentonites [27]; zeolites and amorphous phases in zeolitized tuffaceous rocks [28]; granitic pegmatite [29]; ultramafic rocks [30]; mineral concentrations in bauxite residues [31]; carbonate rocks containing Mg-rich calcite and non-stoichiometric dolomite [32]; hydroxy-interlayered smectite in soils [33].

The Rietveld XRPD method is now considered as the most flexible and accurate one for determination of mineral abundances, especially when examining inhomogeneous rocks containing areas with significant differences in grain size or fine-zoned rocks such as various types of skarns. In general, most skarn minerals (such as garnet, pyroxene, melilite, epidote, olivine, amphibole, plagioclase, etc.) show marked compositional variations not only within one zone but also within an individual crystal due to local heterogeneous skarn formation conditions. In this case, the determination of mineral contents by routine methods (point-counting in thin sections or whole-rock analyses) is not suited. Additionally, X-ray diffraction patterns of skarns are complex, with hundreds of overlapping peaks, which make it difficult to find any peaks suitable for measuring integrated intensities.

The aim of the present paper is to demonstrate the abilities of the Rietveld XRPD method for quantitative determination of minerals in skarn samples from Zvezdel–Pcheloyad Pb–Zn ore deposit (Eastern Rhodopes, Bulgaria), containing chemically variable crystalline phases. This methodology is fast, inexpensive and accurate. Optical study and electron probe microanalysis were performed in order to make comparisons with the Rietveld XRPD results. The obtained data provide important mineralogical information with possibilities for genetic interpretations. The results can be used in petrological studies when quantitative analysis of similar inhomogeneous samples with analogous mineral composition is required.

## 2. Geological Setting

Skarn xenoliths were found to occur in mine gallery No 68 from the Zvezdel–Pcheloyad Pb–Zn ore deposit hosted by monzonitic rocks of the second intrusive phase of the Zvezdel pluton [34]. The Zvezdel pluton is the biggest monzonitic intrusion in the Bulgarian part of the East Rhodopes and is intruded into the comagmatic Paleogene basaltic andesites to trachybasaltic andesites of the Zvezdel volcano. The skarns are zoned, forming bands less than 20 cm in width. The contacts between the different zones are often unclear due to mineralization caused by late stage fluids. The cores of the skarn xenoliths consist of coarse-grained garnet and clinopyroxene–garnet domains in a quartz–calcitic matrix, surrounded

by wollastonite-bearing zones. Based on mineral paragenesis the following zones are determined from the proximal parts of the xenoliths towards the contact with the monzonitic rock: garnet (Grt), clinopyroxene–garnet (Cpx–Grt), plagioclase–clinopyroxene–wollastonite–garnet (Pl–Cpx–Wo–Grt), plagioclase–clinopyroxene–wollastonite (Pl–Cpx–Wo), plagioclase–clinopyroxene–wollastonite–epidote (Pl–Cpx–Wo–Ep), and plagioclase–clinopyroxene (Pl–Cpx). Quartz and calcite are characteristic for all zones. Titanite, apatite, magnetite, and Ti-rich garnets are present as accessory minerals [35].

According to mineral assemblages two main stages of the skarn-forming processes have been distinguished—magmatic (high temperature contact metamorphic) and postmagmatic one [35]. The magmatic stage is represented by melilite (gehlenite 62.5–33.5%, åkermanite 40.6–22.9%, Na-melilite 16.3–4.0%, Fe-åkermanite 10.9–0.1%, Na-Fe<sup>3+</sup>-melilite 10.3–0.0%), “fassaite” clinopyroxene with a high content of the Ca-Tschermak and esseneite components (11.39–17.75 wt% Al<sub>2</sub>O<sub>3</sub>, Fe<sup>3+</sup>—0.180–0.487 apfu), and wollastonite–2M (I generation). The minerals of this stage are observed as relicts in garnets of the postmagmatic stage. The presence of “fassaite” clinopyroxene and melilite suggests high temperature conditions (above 800 °C) in a shallow depth (Phd) before crystallization of the monzonitic magma—estimated by a two-feldspar geothermometer at about 675 °C [34]. The products of this stage are subsequently overprinted by anhydrous metasomatic assemblages of the postmagmatic stage: Ti-rich garnets (TiO<sub>2</sub> content of 8.04–13.10 wt%, schorlomite component—18.95–31.77%), garnets of the grossular–andradite series (Adr<sub>96.61–3.10</sub>), “fassaite” clinopyroxene (II generation), clinopyroxene of the diopside–hedenbergite series (Di<sub>91.17–27.12</sub>), wollastonite–2M (II generation), and plagioclase (Ab<sub>100–3.30</sub>). The wollastonite was determined as 2M polytype using single-crystal XRD structure refinement [36]. Early epidote is also assigned to this stage. The mineral assemblage associated with final phase of hydrothermal activity (retrograde processes) is dominated by late epidote, prehnite, chlorite, fracture-filling thaumasite, gypsum, and zeolite [35].

### 3. Materials and Methods

#### 3.1. Materials

All rock samples used in the present study were collected from the skarn xenoliths from the Zvezdel–Pcheloyad ore deposit. After preliminary X-ray phase analysis, optical and electron microprobe studies of six well-characterized samples were chosen to represent the different skarn zones for quantitative analysis.

#### 3.2. Optical and SEM/EPMA Methods

Polished thin sections were prepared from each sample for examination under optical polarizing microscope. The minerals in the samples were determined by standard optical methods using a Leitz Orthoplan microscope (Ernst Leitz GmbH, Wetzlar, Germany).

The chemical compositions of selected individual phases in each thin section were determined by ZEISS EVO 25LS (Carl Zeiss SMT Ltd, Cambridge, England) scanning electron microscope equipped with an EDAX Trident (AMETEK, EDAX Inc., Mahwah, NJ, USA) system at 16 kV accelerating voltage, about 1 nA beam current, using reference standards.

Optical and electron probe microanalysis (EPMA) were used for precise mineral identification and to compare with the XRPD-derived mineral compositions. Representative EPMA analyses and structural formulae of studied skarn minerals are given in the Appendix A (Tables A1–A7).

#### 3.3. XRPD Data Collection and Rietveld Refinement

The selected samples for quantitative analysis were ground to optimum grain-size for XRPD analysis (<10 µm) and pressed from the bottom of the sample holder in order to minimize partially preferred orientation of anisotropic grains. Step-scan X-ray powder diffraction data was collected over a range of 4–80 2θ with CuKα radiation on D2 Phaser—Bruker AXS Bragg–Brentano diffractometer operated at 30 kV and 10 mA with a step size of 0.02 2θ and a counting time of 4 s/step. The identification

of all minerals was performed using powder diffraction files of the International Centre for Diffraction Data—ICDD, PDF2 database [37].

The phase quantification procedure involved the identification of the mineral phases followed by subsequent quantitative phase analysis of all data sets using the full profile Rietveld method implemented in the FullProf Suite Program, version July 2017 [38–40]. For the samples with more complex mineralogy containing phases with marked anisotropy, we used the Topas v4.2 software [41].

The crystal structure parameters used as starting models of each of the component phases were taken from literature sources (Table 1).

**Table 1.** Sources of crystal structure data used to derive starting models of the minerals for the quantitative phase analysis.

Mineral	Sources of Crystal Structure Data
Albite	Armbruster et al. (1990) [42]
Labradorite	Wenk et al. (1980) [43]
Andradite	Lager et al. (1989) [44]
Grossular	Hasen and Finger (1978) [45]
Diopside	Levien and Prewitt (1981) [46]
Hedenbergite	Cameron et al. (1973) [47]
Esseneite	Cosca and Peacor (1987) [48]
Wollastonite 2M	Hesse (1984) [49]
Epidote	Dollase (1971) [50]
Prehnite	Papike and Zoltai (1967) [51]
Calcite	Effenberger et al. (1981) [52]
Quartz	Levien et al. (1980) [53]
Chlorite	Zanazzi et al. (2009) [54]

The sequence of parameters, which were refined, is the following: scale factors for all phases, zero-shift parameter, background polynomial coefficients, unit-cell parameters for each phase, half-width parameters, atomic site occupancies, atomic coordinates, and preferred orientation. Details of the Rietveld refinement strategy and suggested guidelines are reported by Hill and Madsen [9,55] and Young et al. [56].

A correction for preferred orientation (exponential function implemented in the program Fullprof and preferred orientation spherical harmonics in Topas v4.2 software) was refined for minerals with marked grain-shape anisotropy (feldspars, pyroxene, wollastonite, calcite, epidote, chlorite, etc.). The effect of preferred orientation on the scale factors of the phases is minimized by Rietveld full profile fitting, especially for phases with a large number of XRPD reflexes [13]. The unit cell parameters and the atomic site occupancies of the major minerals with expressed isomorphism were set as variables in the final cycles of refinement (e.g., the Ca and Na content of the feldspars, the Mg and Fe content of the pyroxenes, Al and Fe content of the garnets). The chemical composition determined by EPMA was assigned to the minor minerals present.

The fit of the calculated profile with the measured XRPD pattern gives scale factors for each phase which are related to the weight fractions by Equation (1) [10]:

$$W_p = S_p(ZMV)_p / \sum_i S_i(ZMV)_i \quad (1)$$

where  $S$ ,  $Z$ ,  $M$  and  $V$  are, respectively, the Rietveld scale factor, the number of formula units per unit cell, the mass of the formula unit and the unit-cell volume.

The quality of the fit between the calculated and observed diffraction profiles obtained in a Rietveld refinement is usually given with the standard agreement indices  $R_p$ ,  $R_{wp}$ ,  $R_{exp}$  and the goodness of fit index (GofF), defined by Young et al. [15].

## 4. Results

### 4.1. Garnet Skarn

The garnet zone is dominantly composed of garnets, calcite and quartz with minor prehnite and chlorite. Magnetite, apatite and titanite occur as accessory minerals. The grain-size of the rock varies in a very wide range—from a few microns to 4 mm. Coarse-grained euhedral garnet crystals occur in a fine-grained quartz–calcite–grossular matrix (Figure 1a,b). Due to the presence of fine-grained material, an optical mode was not applicable for this sample.

Based on optical characteristics and electron probe microanalyses, different garnet generations were identified. The earliest garnets are Ti-rich ( $\text{TiO}_2$  from 5.30 wt% to 11.23 wt% and schorlomite component up to 31.8%) and under plane polarized light they appear as brown to red-brown isotropic crystals (Figure 1c,d). The second generation is represented by coarse-grained garnets, which belong to the grossular–andradite solid solution ranging in composition from  $\text{Adr}_{8.5}\text{Grs}_{88.6}$  to almost pure andradite  $\text{Adr}_{94.3}\text{Grs}_{2.8}$  with spessartine, pyrope, almandine, uvarovite, schorlomite, and goldmanite collectively less than 3%. On a local scale, these garnets are continuously zoned with Fe-rich cores and Al-rich rims or exhibit oscillatory zoning, chemically expressed by variations in Al-content. The garnets from the third generation form fine-grained aggregates in the quartz–calcite matrix and are more grossular-rich (grossular component 60–85%).

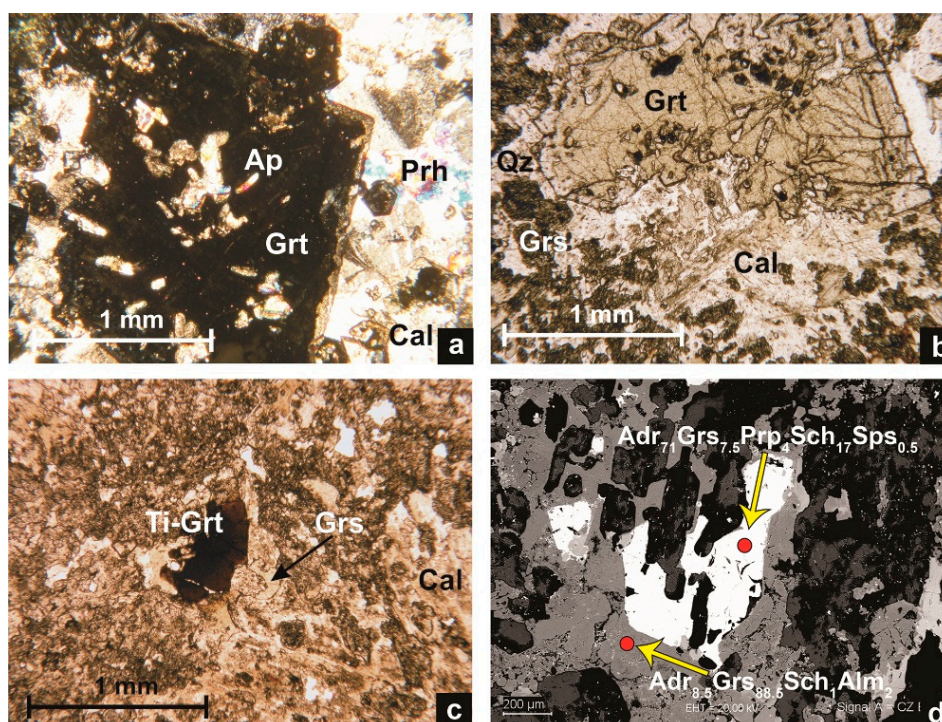


**Figure 1.** Transmitted light photomicrographs of grossular–andradite garnets under crossed polarized light (a) and under plane polarized light (b); (c) Ti-rich garnet in plane polarized light; (d) backscattered electron images of garnet skarn showing a sharp contact between Ti-rich andradite and grossular of later generation. *Abbreviations:* Ap—apatite, Grt—garnet, Prh—pehnite, Cal—calcite, Qz—quartz, Grs—grossular, Ti-Grt—Ti-rich garnet, Adr—andradite, Prp—pyrope, Sch—schorlomite, Sps—spessartine, Alm—almandine.

The mineral composition of garnet skarn determined by XRPD is shown in Figure 2. The peaks of two type of garnets are well resolved in the patterns especially at d-spacing 2.99–2.97 Å, 2.67–2.65 Å. The grossular–andradite in this sample is modeled in the Rietveld analysis as a separate phase from grossular and both phases have unit cell dimensions that allow them to be distinguished in the diffraction patterns. Because of the relatively low abundance, Ti-rich andradite is not included in the refinements. The X-ray Rietveld refinements began with five major phases: quartz, calcite, grossular, grossular–andradite, and chlorite (Figure 3). No traces of the other minor phases could be detected in the diffraction pattern.

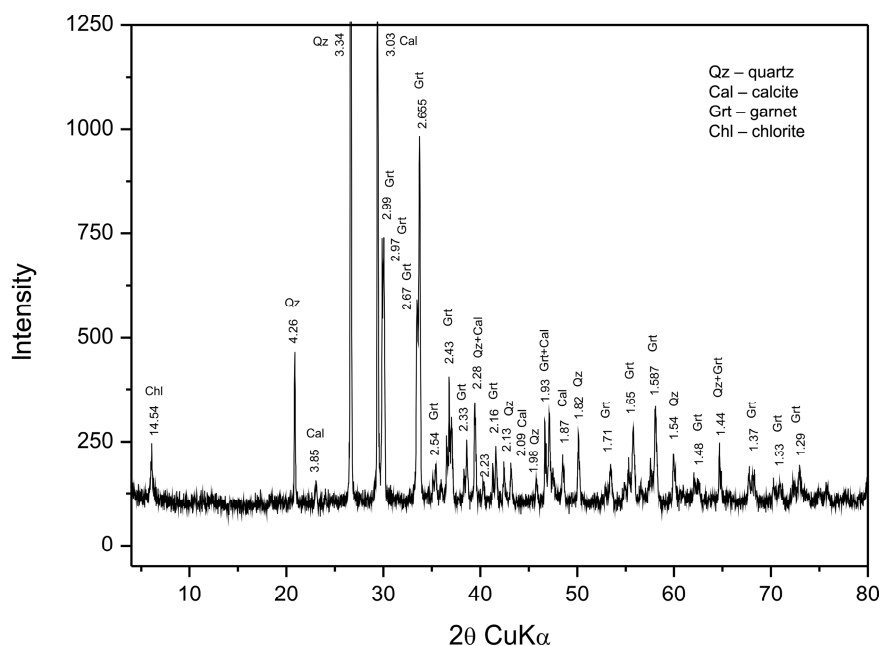


**Figure 2.** X-ray powder diffraction patterns of a garnet skarn (d-spacings of the peaks are indicated).

The sequence of parameters, which were refined, is the following: scale factors for quartz, calcite, grossular, grossular–andradite, chlorite (phases 1, 2, 3, 4 and 5); zero shift, background polynomial parameters (six coefficients); unit cell parameters for all phases; half-width parameters for all phases (U, V, W); atomic site occupancies of Al and Fe in garnets (phases 3 and 4); atomic coordinates of phases 3 and 4; preferred orientation correction for phases 1 and 2.

Visualization of the fit is given in a difference plot on Figure 3. The obtained quantities for the minerals present in the studied sample are (in wt%): quartz—30.41(1), calcite—34.40(3), grossular ( $\text{Ca}_3\text{Al}_{1.8}\text{Fe}_{0.2}\text{Si}_3\text{O}_{12}$ )—21.41(3), grossular–andradite ( $\text{Ca}_3\text{Al}_{0.9}\text{Fe}_{1.1}\text{Si}_3\text{O}_{12}$ )—12.78(4), chlorite—~1(1). The values of the standard agreement indices are  $R_p$ —10.4,  $R_{wp}$ —13.8,  $R_{exp}$ —8.61, GofF—1.6, DW-Stat.—1.14.

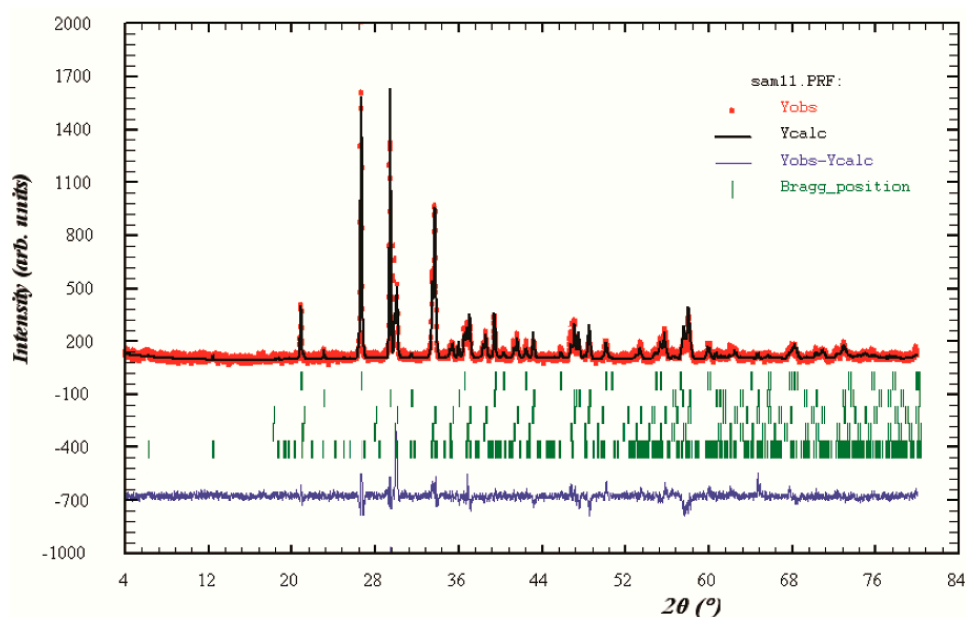


**Figure 3.** Rietveld refinement plot for garnet skarn. The rows of vertical lines give the positions of all possible Bragg reflections for (from top to bottom) quartz, calcite, grossular ( $\text{Ca}_3\text{Al}_2\text{Fe}_0.2\text{Si}_3\text{O}_{12}$ ), grossular-andradite ( $\text{Ca}_3\text{Al}_0.9\text{Fe}_{1.1}\text{Si}_3\text{O}_{12}$ ), and chlorite.

#### 4.2. Clinopyroxene–Garnet Skarn

This is a fine- to coarse-grained rock containing garnets and clinopyroxene in quartz–calcite matrix with minor prehnite and chlorite. Accessory minerals include magnetite, apatite and titanite.

The garnets in this sample, like those in garnet skarn, are represented by at least three generations: Ti-rich garnets, zoned coarse-grained grossular-andradites (Figure 4a), and fine-grained grossular aggregates in quartz–calcite matrix. Grossular–andradites form poikiloblastic crystals that host relict minerals from the early high temperature contact metamorphic stage: melilite (Figure 4d), wollastonite–2M (I generation) (Figure 4c) and “fassaitic” clinopyroxene (I generation). Clinopyroxene of the IInd generation commonly occurs as inclusions in garnet or as crystal aggregates in the quartz–calcite matrix, which exhibit strongly corroded margins. Optically, it shows strong dispersion of the optic axes,  $r > v$ , and displays anomalous blue and brown interference colors (Figure 4b). The chemical compositions of the clinopyroxene from both generations are characterized by significant deficiency of  $\text{SiO}_2$ , (Si 1.32–1.50 apfu) and high contents of esseneite (up to 46%) and Ca-Tschermak (up to 24%) components. Clinopyroxene of the I<sup>st</sup> generation has lower content of esseneite (up to 20%).

The mineral composition of clinopyroxene–garnet skarn determined by XRPD is shown in Figure 5. The grossular–andradite in this sample is modeled in the Rietveld analysis as separate phases from grossular and clinopyroxene as esseneite. The XRPD Rietveld refinements incorporate only the six phases quartz, calcite, grossular, grossular–andradite, chlorite and clinopyroxene. No traces of the other minor phases could be detected in the diffraction pattern. According to optical and SEM studies Ti-rich andradite, melilite and wollastonite occur in quantities that are too small to be detected as discrete phases in the X-ray pattern. Clinopyroxenes from both generations could not be distinguished crystallographically. The sequence of the refined parameters is: scale factors for quartz, calcite, grossular, grossular-andradite, chlorite, clinopyroxene (phases 1, 2, 3, 4, 5, 6); zero shift; background polynomial parameters (six coefficients); unit cell parameters for phases 1, 2, 3, 4, 5, 6; half-width parameters for all phases (U, V, W); atomic site occupancies of Al and Fe in garnets (phases 3 and 4); atomic coordinates of phases 3 and 4; atomic site occupancies of Mg and Fe in clinopyroxene (phase 6) atomic coordinates of phase 6; preferred orientation correction for phases 1, 2 and 6.

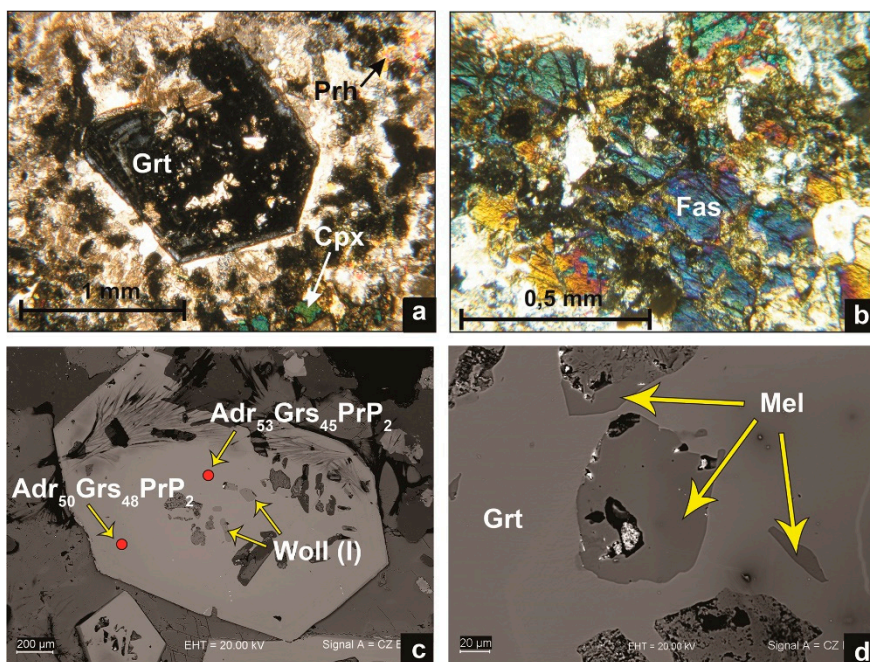


**Figure 4.** (a) Transmitted light photomicrograph of grossular–andradite garnet showing sectorial birefringence in the rim (crossed polarized light); (b) photomicrographs of “fassaitic” clinopyroxene with anomalous blue and brown interference colors (transmitted crossed polarized light); (c) backscattered electron image of wollastonite (I generation) included in grossular–andradite garnet (polished section); (d) backscattered electron image of melilite grains in garnet matrix (polished section). *Abbreviations:* Grt—garnet, Cpx—clinopyroxene, Prh—pehnite, Fas—“fassaitic” clinopyroxene, Woll—wollastonite, Grs—grossular, ADR—andradite, Prp—pyrope, Mel—melilite.

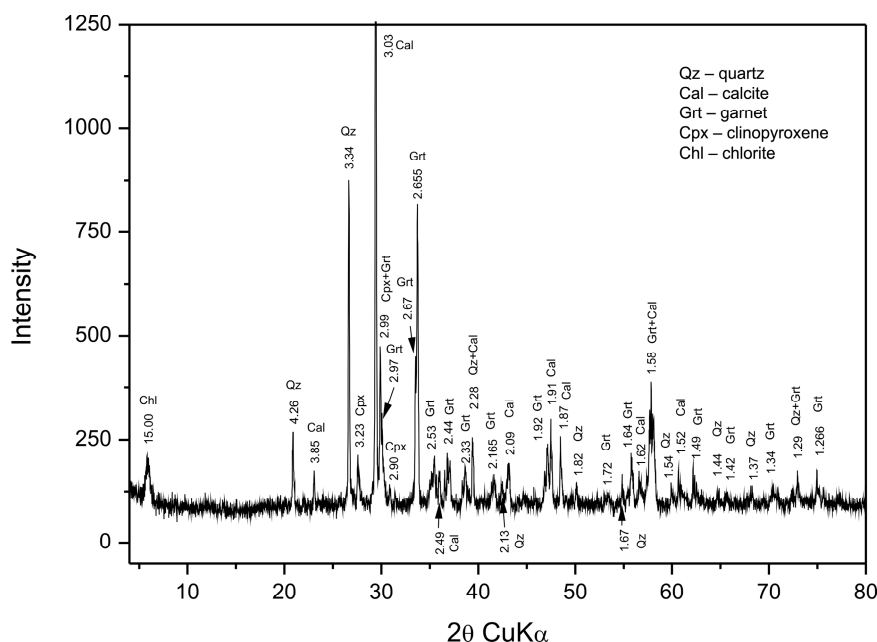


**Figure 5.** X-ray powder diffraction patterns of a clinopyroxene–garnet skarn (d-spacings of the peaks are indicated).

The Rietveld refinement plot of the fit is shown on Figure 6. The obtained mineral quantities in clinopyroxene–garnet skarn are (in wt%): quartz—17.65(2), calcite—41.31(2), grossular (Ca<sub>3</sub>Al<sub>1.8</sub>Fe<sub>0.2</sub>Si<sub>3</sub>O<sub>12</sub>)—18.55(1), grossular–andradite (Ca<sub>3</sub>Al<sub>0.9</sub>Fe<sub>1.1</sub>Si<sub>3</sub>O<sub>12</sub>)—13.46(2), chlorite—~1(1),

clinopyroxene—9.3(3). The values of the standard agreement indices are  $R_p$ —10.3,  $R_{wp}$ —13.9,  $R_{exp}$ —8.49, GofF—1.1, DW-Stat.—1.22.

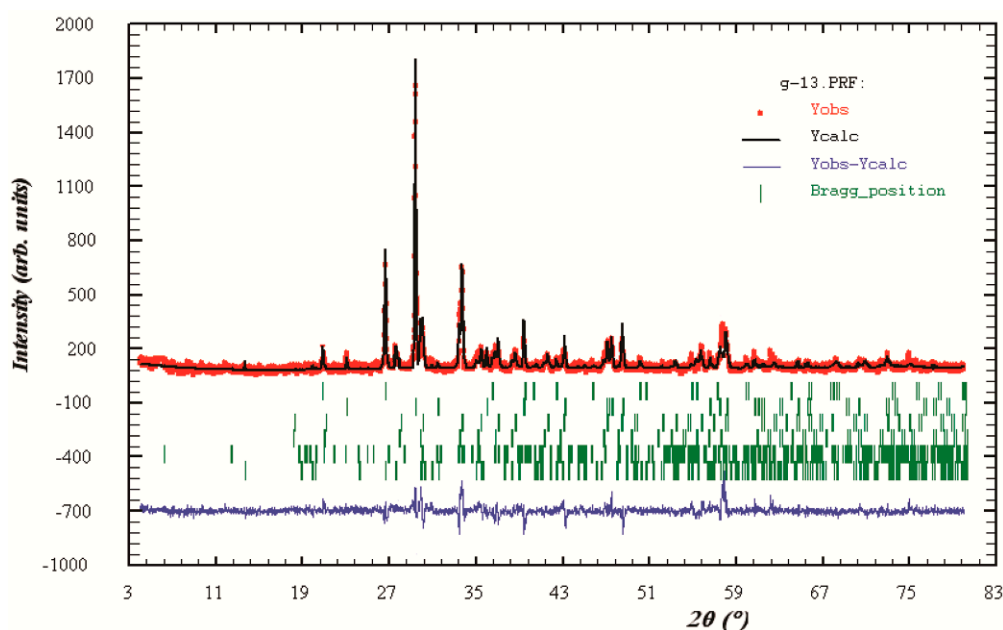


**Figure 6.** Rietveld refinement plot for clinopyroxene–garnet skarn. The rows of vertical lines give the positions of all possible Bragg reflections for (from top to bottom) quartz, calcite, grossular ( $\text{Ca}_3\text{Al}_{1.8}\text{Fe}_{0.2}\text{Si}_3\text{O}_{12}$ ), grossular–andradite ( $\text{Ca}_3\text{Al}_{0.9}\text{Fe}_{1.1}\text{Si}_3\text{O}_{12}$ ), chlorite and clinopyroxene.

#### 4.3. Plagioclase–Clinopyroxene–Wollastonite–Garnet Skarn

The rock is coarse- to fine-grained and contains garnet, wollastonite (II generation), plagioclase, clinopyroxene, and calcite. Minor or secondary minerals present are Ti-rich andradite (Figure 7a), quartz, prehnite, chlorite, and thaumasite. Accessory phases include titanite, apatite and magnetite. All of the constituent minerals are unevenly distributed within the zone. The rock is affected by intense retrograde processes represented by albitisation of former plagioclase, prehnitization of former wollastonite, and fracture-filling thaumasite (Figure 7b,d).

The garnets in this sample are grossular–andradites of intermediate composition (with andradite component from 42% to 50%) (Figure 7c,d), but later almost pure andradite is also found (Figure 7d). EPMA analysis and optical studies identified two types of clinopyroxene: “fassaite” clinopyroxene (esseneite component—up to 50% and Ca-Tschermak—up to 19%) with anomalous blue and brown interference colors and clinopyroxene of the diopside–hedenbergite series (mean  $\text{Wo}_{51}\text{En}_{41}\text{Fs}_8$ ) (Figure 7a).

The mineral composition of Pl-Cpx-Wo-Grt skarn determined by XRPD is shown in Figure 8. The Rietveld analysis starting set of the phases (grossular–andradite, clinopyroxene, plagioclase, wollastonite–2M, and calcite) was based on EPMA (Tables A1–A5), optical, single crystal, and XRPD data. Clinopyroxenes from both types could not be distinguished because of the relatively low abundance of the “fassaite” clinopyroxene and Rietveld analysis began with one pyroxene modeled as diopside–hedenbergite. Plagioclase is modeled as albite, garnet as grossular–andradite with intermediate composition, and wollastonite as wollastonite–2M. The sequence of refined parameters is the following: scale factors for plagioclase, clinopyroxene, calcite, wollastonite–2M, grossular–andradite (phases 1, 2, 3, 4, 5); zero shift, background polynomial parameters (22 coefficients); unit cell parameters for phases 1, 2, 3, 4, 5; half-width parameters for all phases (U, V, W); atomic site occupancies of Al and Fe in garnets (phase 5); atomic coordinates of phase 5; atomic site occupancies of Mg and Fe in clinopyroxene (phase 2); atomic coordinates of phase 2; preferred orientation correction for phases 1, 2, 3 and 4.

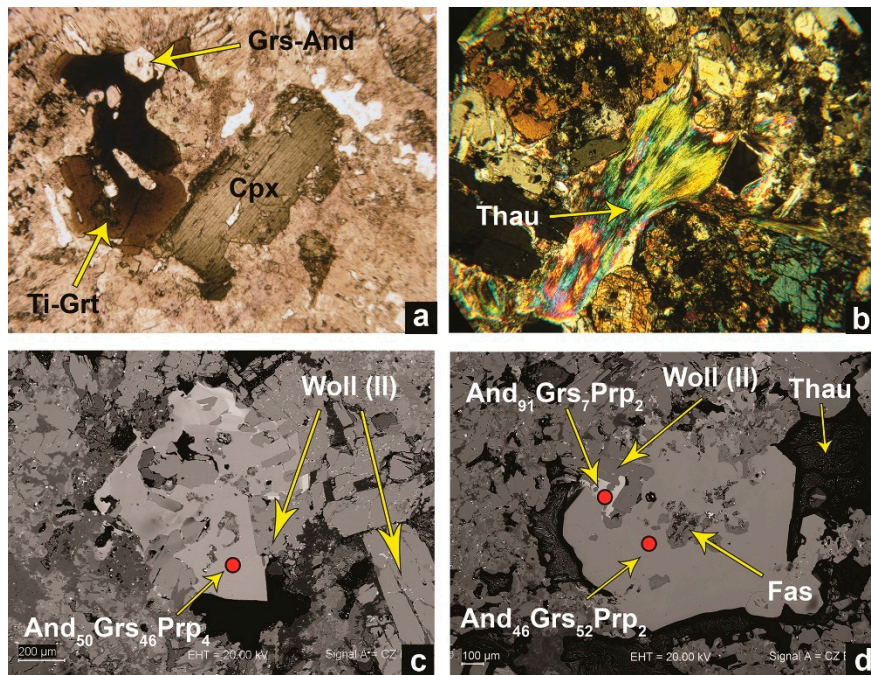


**Figure 7.** (a) Transmitted light photomicrograph showing Ti-rich garnet, grossular–andradite and clinopyroxene of the diopside–hedenbergite series (plane polarized light); (b) photomicrographs thauasite (transmitted crossed polarized light); (c) backscattered electron image of wollastonite (II generation) and grossular–andradite garnet with intermediate composition (polished section); (d) backscattered electron image of “fassaitic” clinopyroxene included in grossular–andradite garnet and later almost pure andradite (polished section). Abbreviations: Ti-Grt—Ti-rich garnet, Grs—grossular, And—andradite, Cpx—clinopyroxene, Fas—“fassaitic” clinopyroxene, Woll—wollastonite, Prp—pyrope, Thau—thauasite.

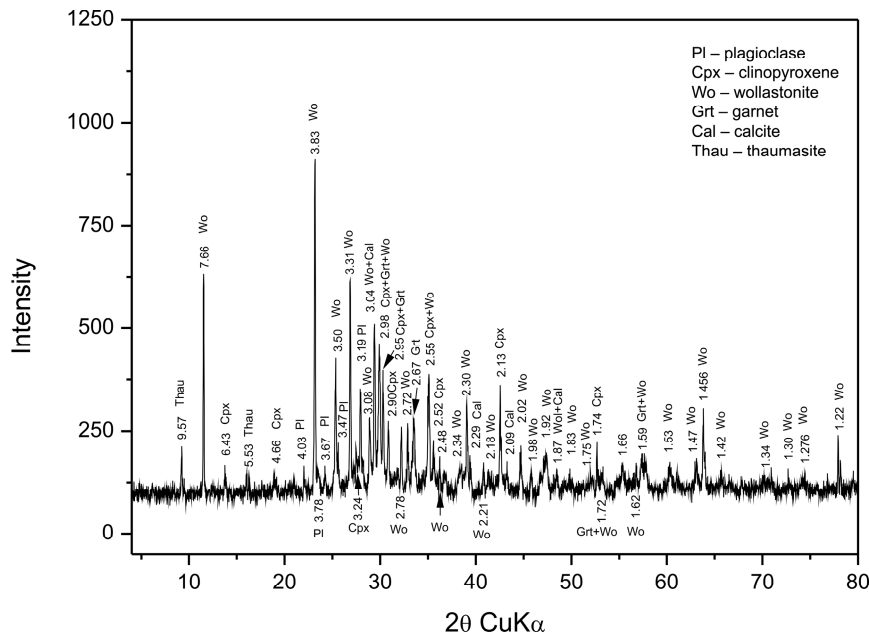


**Figure 8.** X-ray powder diffraction patterns of a PI-Cpx-Wo-Grt skarn (d-spacings of the peaks are indicated).

Figure 9 shows the Rietveld refinement plot for the PI-Cpx-Wo-Grt skarn. The obtained mineral quantities in this sample are (in wt%): plagioclase—46.69(2), clinopyroxene—22.30(1),

wollastonite—15.04(4), grossular–andradite—8.04(2), and calcite—7.93(1). The values of the standard agreement indices are  $R_p$ —18.63,  $R_{wp}$ —21.33,  $R_{exp}$ —17.29, GofF—1.23, DW-Stat.—1.24.

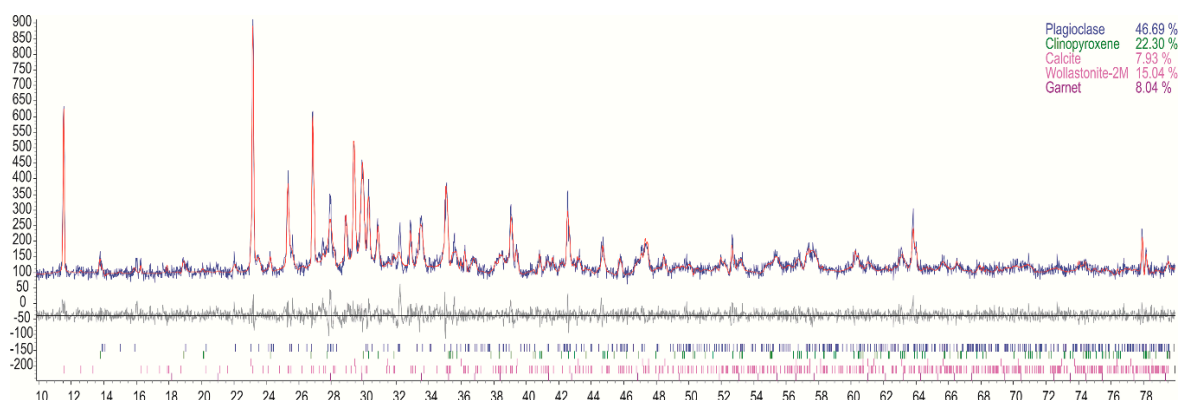


**Figure 9.** Rietveld refinement plots for the Pl-Cpx-Wo-Grt skarn. Above, the measured (blue line) and calculated pattern (red line) are presented, underneath the difference curve is given. Below, the reflection positions of the phases given in the upper right corner are displayed.

#### 4.4. Plagioclase-Clinopyroxene-Wollastonite Skarn

This skarn rock is characterized by significant difference in the grain size of the constituent minerals. Minerals identified in thin section include plagioclase, clinopyroxene, wollastonite (Figure 10a,b) with minor or secondary Ti-rich andradite, calcite, quartz, prehnite, and chlorite. Titanite, apatite and magnetite occur as accessory phases. All of the minerals are unevenly distributed within the zone.

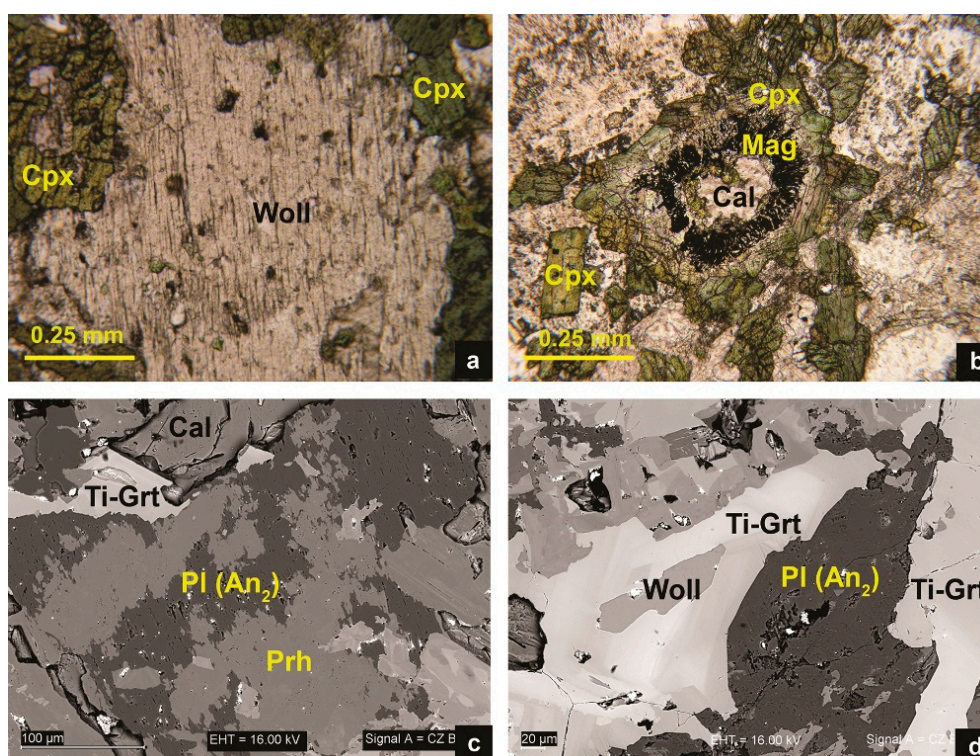


**Figure 10.** (a,b) Transmitted light photomicrographs of Pl-Cpx-Wo skarn (plane polarized light); (c,d) backscattered electron images of Pl-Cpx-Wo skarn. Abbreviations: Woll—wollastonite, Cpx—clinopyroxene, Cal—calcite, Mag—magnetite, Ti-Grt—Ti-rich garnet, Pl—plagioclase, An—anorthite.

The anorthite content in plagioclase in this sample (obtained from EPMA) shows large variations—from 1.9% to 76.4% because plagioclase is partially replaced by albite during the later retrograde processes (Figure 10c,d). The clinopyroxenes in this zone belong to the diopside–hedenbergite series ( $\text{Wo}_{50}\text{En}_{36-39}\text{Fs}_{11-14}$ ). Wollastonite forms coarse poikiloblastic crystals that host clinopyroxene and other rock-forming minerals (Figure 10a). Prehnite occurs in interstitial positions or replaces earlier formed minerals.

The mineral composition of Pl-Cpx-Wo skarn determined by XRPD is shown in Figure 11. The XRPD Rietveld refinement began with five phases: plagioclase, clinopyroxene, wollastonite–2M, calcite and prehnite. According to optical and EPMA (Tables A3–A5 and A7) studies, the plagioclase is modeled as labradorite and clinopyroxene as diopside–hedenbergite. None of the other minor phases could be detected above background. The sequence of refined parameters is the following: scale factors for plagioclase, wollastonite–2M, clinopyroxene, calcite, prehnite (phases 1, 2, 3, 4, 5); zero shift; background polynomial parameters (22 coefficients); unit cell parameters for phases 1, 2, 3, 4, 5; half-width parameters for all phases (U, V, W); atomic site occupancies of Ca and Na in plagioclase (phase 1); atomic coordinates of phase 1; atomic site occupancies of Mg and Fe in clinopyroxene (phase 3); atomic coordinates of phase 3; preferred orientation correction for phases 1, 2, 3, 4, and 5.

Rietveld refinement plot of Pl-Cpx-Wo skarn is given in Figure 12. The obtained mineral quantities in this sample are (in wt%): plagioclase—32.15(3), wollastonite–2M—24.13(1), clinopyroxene—15.58(2), calcite—4.32(2), prehnite—23.81(4). The values of the standard agreement indices are  $R_p$ —13.66,  $R_{wp}$ —15.00,  $R_{exp}$ —13.76, Goff—1.09, DW-Stat.—1.97.

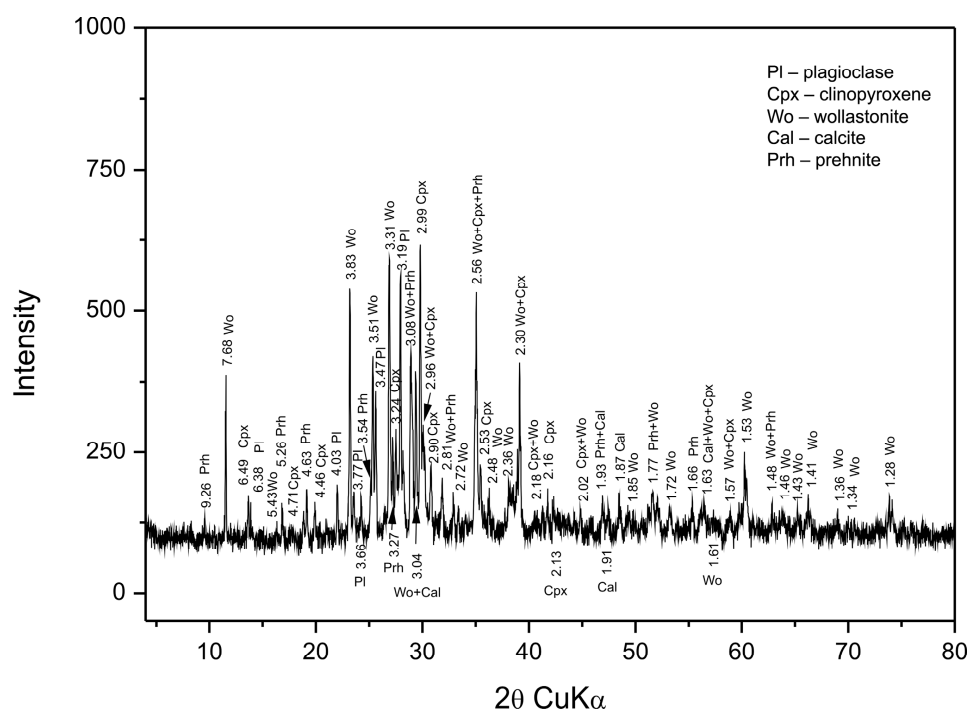
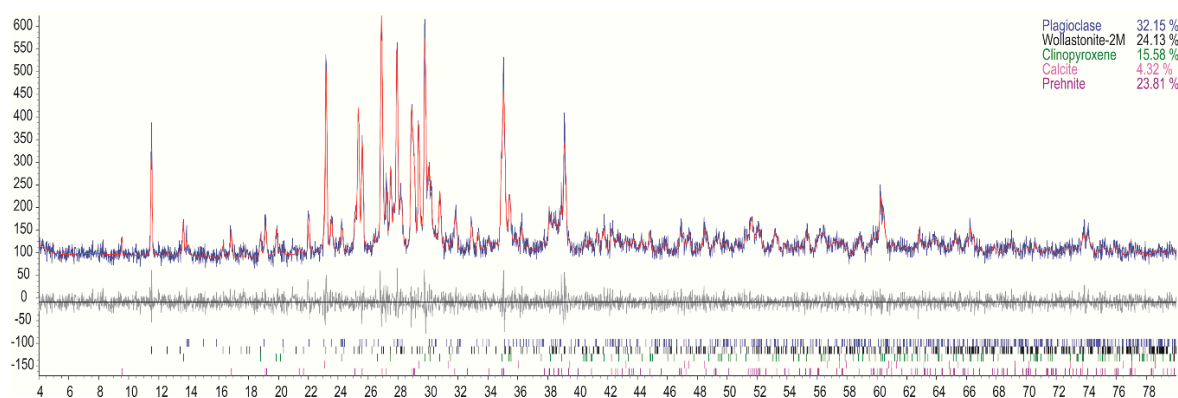


Figure 11. X-ray powder diffraction patterns of Pl-Cpx-Wo skarn (d-spacings are indicated).



**Figure 12.** Rietveld refinement plots for the Pl-Cpx-Wo skarn. Above, the measured (blue line) and calculated pattern (red line) are presented, underneath the difference curve is given. Below, the reflection positions of the phases given in the upper right corner are displayed.

#### 4.5. Plagioclase-Clinopyroxene-Wollastonite-Epidote Skarn

Pl-Cpx-Wo-Ep skarn is dominated by plagioclase, clinopyroxene, wollastonite, with subordinate ore minor epidote, calcite, quartz, chlorite, prehnite, and Ti-rich andradite, grossular-andradite (Figure 13a,d). Accessory minerals are titanite, apatite and magnetite. The rock is coarse- to fine-grained and characterized by unevenly distribution of the constituent minerals.

According to EPMA and optical data, the mean content of the anorthite component in plagioclase is about 58%. Usually the primary plagioclase is partially replaced by albite. The clinopyroxenes in this zone belong to the diopside–hedenbergite series ( $\text{Di}_{36-80}\text{Hd}_{21-63}$ ). The  $\text{Fe}^{3+}/(\text{Fe}^{3+} + \text{Al})$  ratio in the epidote composition ranges from 0.16 to 0.32. Locally, titanite forms porphyroblasts up to 1 mm long (Figure 13c). Prehnite occurs in interstitial positions or replaces the earlier formed plagioclase and wollastonite.

The mineral composition of Pl-Cpx-Wo-Ep skarn determined by XRPD is presented in Figure 14. The XRPD Rietveld refinements incorporate eight phases: plagioclase, clinopyroxene, wollastonite–2M, calcite, epidote, prehnite, quartz, and chlorite. According to optical and EPMA (Tables A3–A7) studies the plagioclase is modeled as labradorite and clinopyroxene as diopside–hedenbergite. No traces of other minor phases could be detected in the diffraction pattern. The sequence of refined parameters is: scale factors for plagioclase, clinopyroxene, calcite, quartz, chlorite, wollastonite–2M, prehnite, epidote (phases 1, 2, 3, 4, 5, 6, 7, 8); zero shift; background polynomial parameters (22 coefficients); unit cell parameters for all phases; half-width parameters for all phases ( $U, V, W$ ); atomic site occupancies of Ca and Na in plagioclase (phase 1); atomic coordinates of phase 1; atomic site occupancies of Mg and Fe in clinopyroxene (phase 2); atomic coordinates of phase 2; atomic site occupancies of Al and Fe in epidote (phase 8); atomic coordinates of phase 8; preferred orientation correction for phases 1, 2, 3, 5, 6, 7 and 8.

Rietveld refinement plot showing visually the quality of the fits for the Pl-Cpx-Wo-Ep skarn is given in Figure 15. The obtained results for mineral quantities in the sample are (in wt%): plagioclase—47.08(2), clinopyroxene—34.81(1), wollastonite–2M—5.01(3), calcite—3.84(2), epidote—2.33(4), prehnite—2.78(2), quartz—1.67(1), and chlorite—2.49(2). The values of the standard indices of agreement are  $R_p$ —16.28,  $R_{wp}$ —18.36,  $R_{exp}$ —14.91, Goff—1.23, DW-Stat.—1.65.

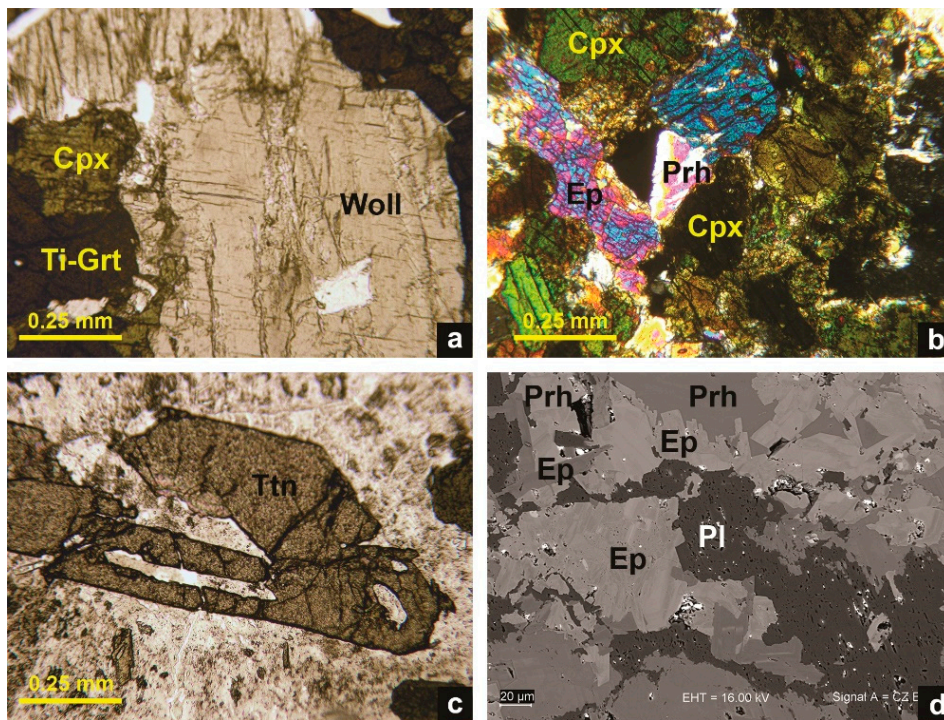


**Figure 13.** Transmitted light photomicrographs of PI-Cpx-Wo-Ep skarn under plane polarized light (a) and (b) under crossed polarized light; (c) photomicrograph of titanite crystal (plane polarized light); (d) backscattered electron images of PI-Cpx-Wo-Ep skarn (polished section). Abbreviations: Woll—wollastonite, Cpx—clinopyroxene, Prh—prehnite, Ttn—titanite; Ti-Grt—Ti-rich garnet, Pl—plagioclase, Ep—epidote.

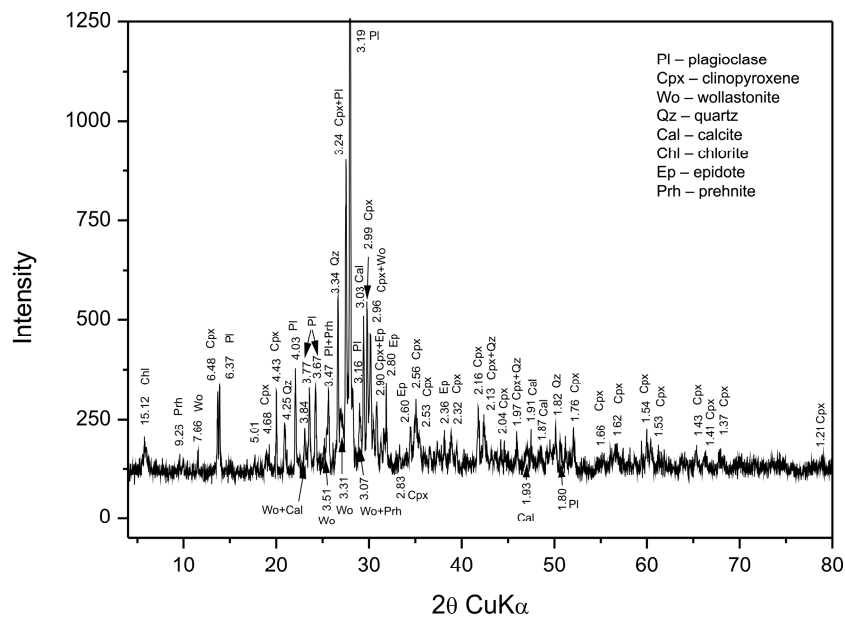


**Figure 14.** X-ray powder diffraction patterns of PI-Cpx-Wo-Ep skarn (d-spacings are indicated).

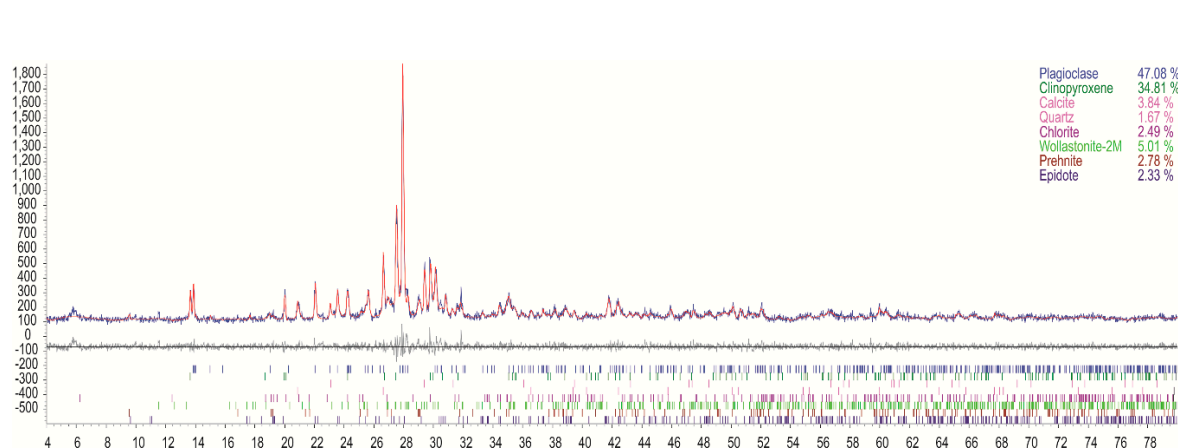


**Figure 15.** Rietveld refinement plots for the Pl-Cpx-Wo-Ep skarn. Above, the measured (blue line) and calculated pattern (red line) are presented, underneath the difference curve is given. Below, the reflection positions of the phases given in the upper right corner are displayed.

#### 4.6. Plagioclase-Clinopyroxene Skarn

This skarn is present close to monzonitic rocks in contact with the skarn xenoliths. The rock is medium-grained and contains plagioclase and clinopyroxene (Figure 16a) with minor or secondary calcite, quartz, prehnite, and chlorite. Accessory minerals include titanite, apatite and magnetite.

Usually the primary plagioclase is partially replaced by albite or prehnite (Figure 16b–d). The mean plagioclase composition measured by EPMA is An<sub>60</sub>. The clinopyroxene in this zone belongs to the diopside–hedenbergite series (Di<sub>48–73</sub>Hd<sub>25–49</sub>Jhn<sub>0–2</sub>) and forms zoned crystals with Mg-rich cores and Fe-rich rims (Figure 16c,d). Prehnite occurs in interstitial positions or replaces the earlier formed plagioclase.

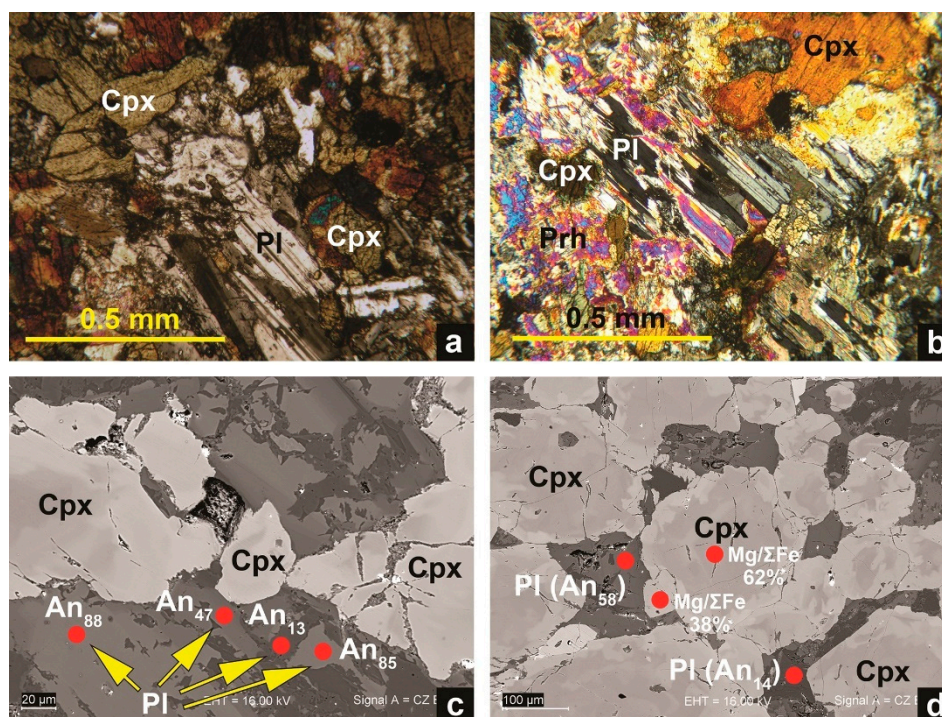


**Figure 16.** Transmitted light photomicrographs of Pl-Cpx skarn under plane polarized light (a) and (b) under crossed polarized light; (c,d) backscattered electron images of Pl-Cpx skarn showing the zoned clinopyroxene crystals with Mg-rich cores and Fe-rich rims (polished section). Abbreviations: Cpx—clinopyroxene, Pl—plagioclase, Prh—prehnite, An—anorthite.

The mineral composition of Pl-Cpx skarn determined by XRPD is shown in Figure 17. The XRPD Rietveld refinements include five phases: plagioclase, clinopyroxene, calcite, quartz, and chlorite. Based on optical and EPMA (Tables A3 and A5) studies, the plagioclase is modeled as labradorite and clinopyroxene as diopside–hedenbergite. The minor phases are present only at the 0–2 vol.% level and could not be detected in the XRPD pattern. The obtained mean plagioclase composition is in agreement both with the mean of the optical determinations and with those measured by EPMA. The sequence of refined parameters is the following: scale factors for plagioclase, clinopyroxene, calcite, quartz, chlorite (phases 1, 2, 3, 4, 5); zero shift, background polynomial parameters (22 coefficients); unit cell parameters for phases 1, 2, 3, 4, 5; half-width parameters for all phases (U, V, W); atomic site occupancies of Ca and Na in plagioclase (phase 1); atomic coordinates of phase 1; atomic site occupancies of Mg and Fe in clinopyroxene (phase 2); atomic coordinates of phase 2; preferred orientation correction for phases 1, 2 and 3.

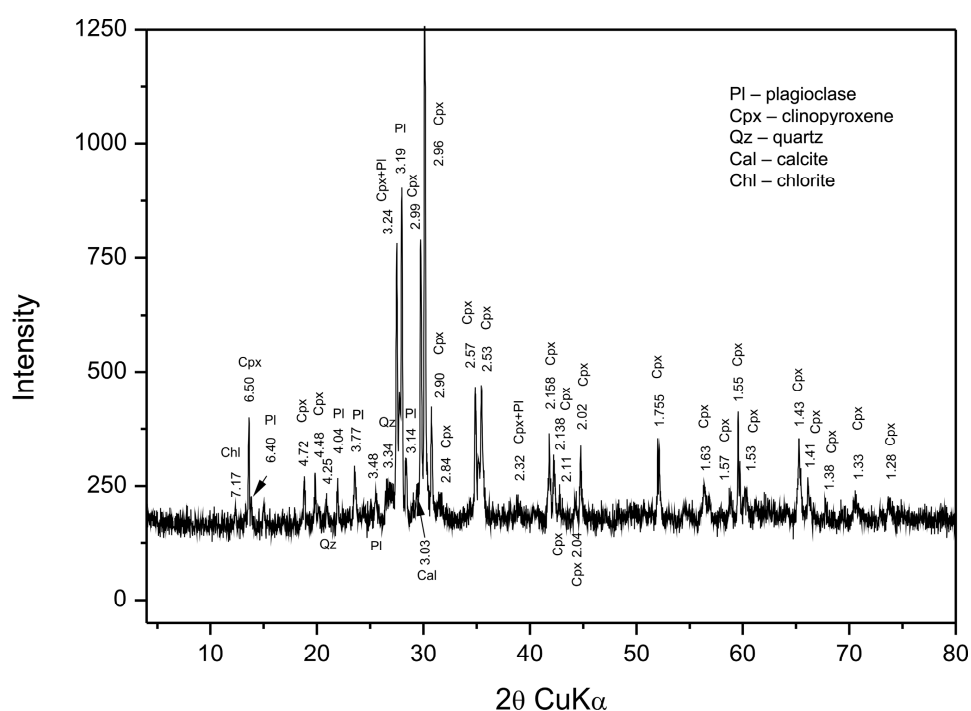


**Figure 17.** X-ray powder diffraction patterns of Pl-Cpx skarn (d-spacings are indicated).

Rietveld refinement plot for the Pl-Cpx skarn is shown in Figure 18. The obtained results for mineral quantities in the sample are (in wt%): plagioclase—41.16(3), clinopyroxene—40.69(5), calcite—14.15(2), quartz—1.29(2), and chlorite—2.72(1). The values of the standard indices of agreement are  $R_p$ —16.76,  $R_{wp}$ —16.37,  $R_{exp}$ —14.04,  $GofF$ —1.17,  $DW$ -Stat.—1.65.

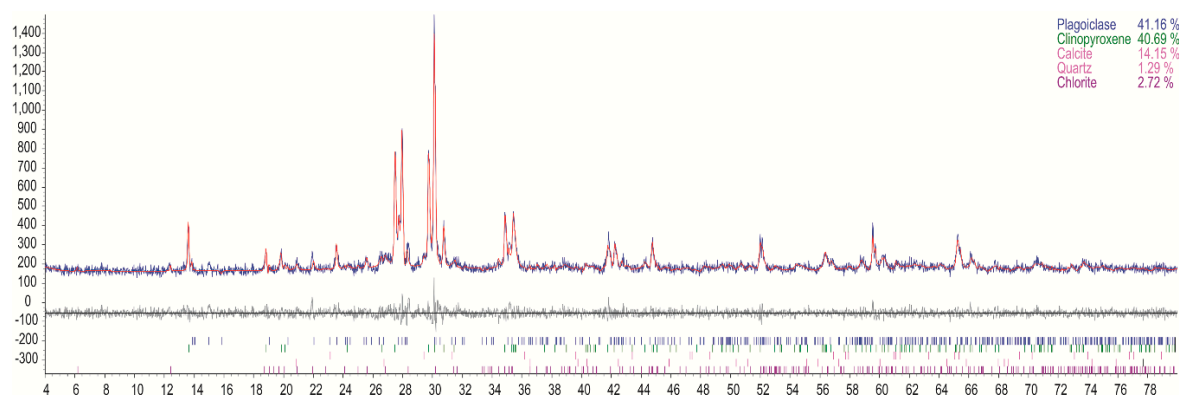


**Figure 18.** Rietveld refinement plots for the Pl-Cpx skarn. Above, the measured (blue line) and calculated pattern (red line) are presented, underneath the difference curve is given. Below, the reflection positions of the phases given in the upper right corner are displayed.

## 5. Discussion

The quantitative analysis of the studied skarn samples showed that the Rietveld method combined with optical and EPMA studies is a suitable approach for quantification of mineral concentrations. This combination of methods was applied in previous studies to improve the quantitative determination of minerals [18–20,24,25].

The studied skarn rocks are inhomogeneous, locally very fine-zoned, containing mineral assemblages from different stages of the skarn processes. In addition, they consist of areas with significant differences in grain size—from fine- to very coarse-grained. The presence of minerals with highly variable mineralogical compositions and chemically zoned crystals further complicate the determination of phase quantities. In this case, the estimation of mineral content by routine methods such as point-counting in thin sections or whole-rock analyses are inappropriate.

When developing a Rietveld XRPD quantification method, a knowledge of mineralogy and crystal structure is important factor for the starting set of the phases. The refined crystal-structure parameters included the unit-cell parameters of each phase and element substitutions with pronounced influences on intensities and positions of the reflections. Atomic positions and site occupancies can be successfully varied for major phases to obtain accurate scale factors. For instance, the  $\text{Ca}^{2+}$  and  $\text{Na}^{+}$  occupancy in plagioclase structure; the  $\text{Ca}^{2+}$ ,  $\text{Mg}^{2+}$ ,  $\text{Fe}^{2+}$ ,  $\text{Al}^{3+}$   $\text{Fe}^{3+}$  occupancy of the octahedral and tetrahedral positions in the clinopyroxene structure; the  $\text{Ca}^{2+}$ ,  $\text{Fe}^{2+}$ ,  $\text{Fe}^{3+}$ ,  $\text{Al}^{3+}$ , and  $\text{Ti}^{4+}$  occupancy of the eight-coordinated dodecahedral, 6-coordinated octahedral, and tetrahedral positions in garnet structure; the  $\text{Mg}^{2+}$  and  $\text{Fe}^{2+}$  occupancy of the octahedral positions in the chlorite structure; the  $\text{Fe}^{3+}$  and  $\text{Al}^{3+}$  occupancy in M3 octahedral position in epidote structure.

The results of some refined parameters of the minerals from the studied skarn samples are presented in Tables 2–7. The derived garnet compositions of grossular and grossular–andradite of the garnet skarn by Rietveld XRPD method are in good agreement with the data of the EPMA measurements (Tables 2 and A1).

The refined unit cell parameters of the “fassaite” type clinopyroxene from the clinopyroxene–garnet skarn are very close to those in the starting model [48] and the compositions of the garnets and clinopyroxene are in accordance with the EPMA data (Tables 3, A1 and A2).

The comparison of the XRPD results with the EPMA analyses of the garnet, clinopyroxene and plagioclase compositions from Pl-Cpx-Wo-Grt skarn (Tables 4, A1, A3 and A5) shows good agreement, given the presence of diopside–hedenbergite and grossular–andradite solid solutions and albite, respectively. The refined unit cell parameters of the wollastonite–2M for all samples are very close to those reported by Hesse [49] (Tables 4–6).

Table 5 presents refined parameters of the minerals from the Pl-Cpx-Wo skarn. The average plagioclase composition of  $\text{An}_{40}$  derived by XRPD is slightly deficient in Ca relative to the mean

value obtained by EPMA (Table A5) but the pyroxene composition is well determined by XRPD, given the presence of cation isomorphous substitution in M1 site in the crystal structure (Tables 5 and A3). The refined unit cell parameters of prehnite in the Pl-Cpx-Wo and Pl-Cpx-Wo-Ep skarns are close to those in the starting model [51].

**Table 2.** Some refined parameters in the quantitative analysis of the garnet skarn and chemical compositions of garnets determined by X-ray powder diffraction (XRPD) and electron probe microanalysis (EPMA).

Minerals	Unit Cell Parameters (Å)		Chemical Compositions	
	starting model	after refinement	XRPD	EPMA
Grossular	$a = 11.846(1)$ [45]	$a = 11.892(2)$	$\text{Ca}_3(\text{Al}_{1.8}, \text{Fe}^{3+}_{0.2})_2\text{Si}_3\text{O}_{12}$	$(\text{Ca}_{2.96-2.98}, \text{Fe}^{2+}_{0-0.04}\text{Mg}_{0-0.1})_3(\text{Al}_{1.66-1.81}, \text{Fe}^{3+}_{0.17-0.26}\text{Ti}_{0-0.01}, \text{Fe}^{2+}_{0-0.01})_2(\text{Si}, \text{Al})_3\text{O}_{12}$
Grossular-andradite	$a = 12.057$ [44]	$a = 11.966(2)$	$\text{Ca}_3(\text{Al}_{0.9}\text{Fe}_{1.1})_2\text{Si}_3\text{O}_{12}$	$(\text{Ca}_{2.95-3.0}, \text{Mg}_{0.01-0.08})_3(\text{Al}_{0.77-0.95}, \text{Fe}^{3+}_{0.95-1.17}\text{Ti}_{0-0.07}, \text{Fe}^{2+}_{0-0.01})_2(\text{Si}, \text{Al})_3\text{O}_{12}$

**Table 3.** Some refined parameters in the quantitative analysis of the clinopyroxene–garnet skarn and chemical compositions of the minerals determined by XRPD and EPMA.

Minerals	Unit Cell Parameters (Å)		Chemical Compositions	
	starting model	after refinement	XRPD	EPMA
Grossular	$a = 11.846(1)$ [45]	$a = 11.873(5)$	$\text{Ca}_3(\text{Al}_{1.8}, \text{Fe}^{3+}_{0.2})_2\text{Si}_3\text{O}_{12}$	$(\text{Ca}_{2.92-3.00}, \text{Mg}_{0.05-0.09})_3(\text{Al}_{1.58-1.80}, \text{Fe}^{3+}_{0.12-0.30}\text{Fe}^{2+}_{0-0.06})_2(\text{Si}, \text{Al})_3\text{O}_{12}$
Grossular-andradite	$a = 12.057$ [44]	$a = 11.952(4)$	$\text{Ca}_3(\text{Al}_{0.9}\text{Fe}_{1.1})_2\text{Si}_3\text{O}_{12}$	$(\text{Ca}_{2.93-3.00}, \text{Mg}_{0-0.07})_3(\text{Al}_{0.78-0.94}, \text{Fe}^{3+}_{1.00-1.10}, \text{Ti}_{0-0.05})_2(\text{Si}, \text{Al})_3\text{O}_{12}$
Clinopyroxene	$a = 9.79(1)$ [48] $b = 8.822(9)$ $c = 5.37(1)$ $\beta = 105.81(9)$	$a = 9.77(1)$ $b = 8.83(1)$ $c = 5.36(6)$ $\beta = 105.78(1)$	$\text{Ca}(\text{Mg}_{0.40}\text{Fe}^{3+}_{0.40}\text{Al}_{0.20})(\text{Si}_{1.4}, \text{Al}_{0.6})_2\text{O}_6$	$\text{Ca}(\text{Mg}_{0.26-0.47}, \text{Fe}^{3+}_{0.31-0.44}, \text{Al}^{\text{VI}}_{0.10-0.18}, \text{Fe}^{2+}_{0-0.14}, \text{Ti}_{0.02-0.08})(\text{Si}_{1.32-1.48}, \text{Al}^{\text{IV}}_{0.52-0.68})\text{O}_6$

**Table 4.** Some refined parameters in the quantitative analysis of the Pl-Cpx-Wo-Grt skarn and chemical compositions of the minerals determined by XRPD and EPMA.

Minerals	Unit Cell Parameters (Å)		Chemical Compositions	
	starting model	after refinement	XRPD	EPMA
Grossular-andradite	$a = 12.057$ [44]	$a = 11.962(3)$	$\text{Ca}_3(\text{Al}_{0.9}\text{Fe}_{1.1})_2\text{Si}_3\text{O}_{12}$	$(\text{Ca}_{2.91-2.95}, \text{Mg}_{0.06-0.09}, \text{Fe}^{2+}_{0-0.02})_3(\text{Al}_{0.70-1.07}, \text{Fe}^{3+}_{0.85-1.28}, \text{Ti}_{0.01-0.06}, \text{Fe}^{2+}_{0-0.02})_2(\text{Si}, \text{Al})_3\text{O}_{12}$
Clinopyroxene	$a = 9.7456$ [46] $b = 8.9198$ $c = 5.2516$ $\beta = 105.86$	$a = 9.789(3)$ $b = 8.928(3)$ $c = 5.260(2)$ $\beta = 105.77(1)$	$\text{Ca}(\text{Mg}_{0.60}\text{Fe}^{2+}_{0.40})\text{Si}_2\text{O}_6$	$\text{Ca}(\text{Mg}_{0.59-0.92}, \text{Fe}^{2+}_{0.03-0.31}, \text{Fe}^{3+}_{0-0.16}, \text{Al}_{0-0.03})(\text{Si}_{1.85-2.00}, \text{Al}_{0-0.13})_2\text{O}_6$
Plagioclase	$a = 8.137$ [42] $b = 12.785$ $c = 7.1583$ $\alpha = 94.26$ $\beta = 116.60$ $\gamma = 87.71$	$a = 8.140(2)$ $b = 12.780(4)$ $c = 7.152(2)$ $\alpha = 94.176(2)$ $\beta = 116.562(2)$ $\gamma = 87.90(1)$	$\text{Na}_4\text{Al}_4\text{Si}_{12}\text{O}_{32}$	$\text{Na}_{3.92-4.0}\text{Ca}_{0-0.1}\text{K}_{0-0.04}, \text{Fe}^{3+}_{0-0.03}\text{Al}_{3.98-4.0}\text{Si}_{11.95-11.97}\text{O}_{32}$
Wollastonite	$a = 15.409$ [49] $b = 7.322$ $c = 7.063$ $\beta = 95.30$	$a = 15.413(2)$ $b = 7.336(5)$ $c = 7.070(3)$ $\beta = 95.24(5)$	$\text{Ca}_2\text{Si}_2\text{O}_6$	$\text{Ca}_{1.92-1.96}\text{Mg}_{0-0.03}\text{Fe}^{2+}_{0.02-0.03}, (\text{Si}_{1.96-1.99}\text{Al}_{0.04-0.05})\text{O}_6$

**Table 5.** Some refined parameters in the quantitative analysis of the Pl-Cpx-Wo skarn and chemical compositions of the minerals determined by XRPD and EPMA.

Minerals	Unit Cell Parameters (Å)		Chemical Compositions	
	starting model	after refinement	XRPD	EPMA
Clinopyroxene	$a = 9.7456$ [46] $b = 8.9198$ $c = 5.2516$ $\beta = 105.86$	$a = 9.750(3)$ $b = 8.916(2)$ $c = 5.258(1)$ $\beta = 105.99(2)$	$\text{Ca}(\text{Mg}_{0.70}\text{Fe}^{2+}_{0.30})\text{Si}_2\text{O}_6$	$\text{Ca}_{0.99-1.0}\text{Na}_{0.01}(\text{Mg}_{0.65-0.72}\text{Fe}^{2+}_{0.21-0.25}\text{Fe}^{3+}_{0-0.06}\text{Al}_{0-0.04}\text{Cr}_{0-0.005}\text{Mn}_{0.01-0.07})(\text{Si}_{1.96-1.99}\text{Al}_{0.01-0.04})_2\text{O}_6$
Plagioclase	$a = 8.1736$ [43] $b = 12.8736$ $c = 7.1022$ $\alpha = 93.462$ $\beta = 116.054$ $\gamma = 90.475$	$a = 8.150(2)$ $b = 12.790(5)$ $c = 7.140(1)$ $\alpha = 94.185(2)$ $\beta = 116.5432(3)$ $\gamma = 88.81(1)$	$\text{Na}_{2.4}\text{Ca}_{1.6}\text{Al}_4\text{Si}_{12}\text{O}_{32}$	$\text{Na}_{0.99-3.92}\text{Ca}_{0.07-2.50}\text{K}_{0-0.5}\text{Mg}_{0-0.18}\text{Fe}^{3+}_{0-0.05}\text{Al}_{4.03-7.5}\text{Si}_{8.86-12}\text{O}_{32}$
Wollastonite	$a = 15.409$ [49] $b = 7.322$ $c = 7.063$ $\beta = 95.30$	$a = 15.409(7)$ $b = 7.320(3)$ $c = 7.063(2)$ $\beta = 95.36(3)$	$\text{Ca}_2\text{Si}_2\text{O}_6$	$\text{Ca}_{1.97-1.99}\text{Mg}_{0-0.02}\text{Fe}^{2+}_{0.02}\text{Cr}_{0-0.005}\text{Mn}_{0-0.05}(\text{Si}_{1.98-1.99}\text{Al}_{0-0.02})\text{O}_6$
Prehnite	$a = 4.646$ [51] $b = 5.483$ $c = 18.486$	$a = 4.640(2)$ $b = 5.482(2)$ $c = 18.485(7)$	$\text{Ca}_2\text{AlSi}_3\text{O}_{10}(\text{OH})_2$	$\text{Ca}_{1.96-1.98}\text{Fe}^{3+}_{0.01-0.18}\text{Ti}_{0-0.02}\text{Al}_{1.80-1.96}\text{Si}_3\text{O}_{10}(\text{OH})_2$

The refined crystal chemical parameters of the minerals from the Pl-Cpx-Wo-Ep skarn are shown in Table 6. The derived by XRPD mean plagioclase composition after refinement is in agreement both with the mean of the optical determinations and with those measured by EPMA (Table A5). The compositions of the clinopyroxene and the epidote are in good accordance with those determined by EPMA analyses (Tables A3 and A6).

The results for Pl-Cpx skarn after refinements are presented in Table 7. The variation of the Na/Ca content of the plagioclase during the XRPD refinement provided a composition of  $\sim\text{An}_{50}$ , in agreement with optical and EPMA data (Table A5). The pyroxene composition is in agreement with the EPMA results (Table A5).

**Table 6.** Some refined parameters in the quantitative analysis of the Pl-Cpx-Wo-Ep skarn and chemical compositions of the minerals determined by XRPD and EPMA.

Minerals	Unit Cell Parameters (Å)		Chemical Compositions	
	starting model	after refinement	XRPD	EPMA
Clinopyroxene	$a = 9.7456$ [46] $b = 8.9198$ $c = 5.2516$ $\beta = 105.86$	$a = 9.752(2)$ $b = 8.919(2)$ $c = 5.262(7)$ $\beta = 106.10(1)$	$\text{Ca}(\text{Mg}_{0.60}\text{Fe}^{2+}_{0.40})\text{Si}_2\text{O}_6$	$\text{Ca}(\text{Mg}_{0.45-0.67}\text{Fe}^{2+}_{0.23-0.44}\text{Fe}^{3+}_{0.04-0.14}\text{Al}_{0.01-0.06}\text{Ti}_{0.01-0.03})(\text{Si}_{1.79-1.89}\text{Al}_{0.11-0.21})_2\text{O}_6$
Plagioclase	$a = 8.1736$ [43] $b = 12.8736$ $c = 7.1022$ $\alpha = 93.462$ $\beta = 116.054$ $\gamma = 90.475$	$a = 8.167(3)$ $b = 12.864(1)$ $c = 7.122(1)$ $\alpha = 93.625(2)$ $\beta = 116.44(7)$ $\gamma = 89.87(2)$	$\text{Na}_{1.8}\text{Ca}_{2.1}\text{Al}_5\text{Si}_{12}\text{O}_{32}$	$\text{Na}_{0.13-3.24}\text{Ca}_{0.50-3.77}\text{K}_{0-0.11}\text{Fe}^{3+}_{0-0.15}\text{Al}_{4.31-7.41}\text{Si}_{8.40-11.70}\text{O}_{32}$
Wollastonite	$a = 15.409$ [49] $b = 7.322$ $c = 7.063$ $\beta = 95.30$	$a = 15.377(1)$ $b = 7.299(4)$ $c = 7.049(5)$ $\beta = 95.34(6)$	$\text{Ca}_2\text{Si}_2\text{O}_6$	$\text{Ca}_{1.83-1.99}\text{Mg}_{0-0.03}\text{Fe}^{2+}_{0.02-0.05}\text{Cr}_{0-0.005}\text{Ti}_{0-0.06}(\text{Si}_{1.99-2.00}\text{Al}_{0-0.01})\text{O}_6$
Prehnite	$a = 4.646$ [51] $b = 5.483$ $c = 18.486$	$a = 4.640(2)$ $b = 5.482(2)$ $c = 18.485(7)$	$\text{Ca}_2\text{AlSi}_3\text{O}_{10}(\text{OH})_2$	$\text{Ca}_{1.93-2.00}\text{Fe}^{3+}_{0.16-0.38}\text{Al}_{1.60-1.78}\text{Si}_3\text{O}_{10}(\text{OH})_2$
Epidote	$a = 8.914$ [50] $b = 5.640$ $c = 10.162$ $\beta = 115.4$	$a = 8.897(1)$ $b = 5.635(7)$ $c = 10.152(1)$ $\beta = 115.378(4)$	$\text{Ca}_2(\text{Al}_2\text{Fe}^{3+})[\text{Si}_2\text{O}_7][\text{SiO}_4]\text{O}(\text{OH})$	$\text{Ca}_{2.98-2.39}(\text{AlFe}^{3+}_{0.49-0.96})[\text{Si}_2\text{O}_7][\text{SiO}_4]\text{O}(\text{OH})$

**Table 7.** Some refined parameters in the quantitative analysis of the Pl-Cpx skarn and chemical compositions of the minerals determined by XRPD and EPMA.

Minerals	Unit Cell Parameters (Å)		Chemical Compositions	
	starting model	after refinement	XRPD	EPMA
Clinopyroxene	$a = 9.7456$ [46]	$a = 9.745(1)$	$\text{Ca}(\text{Mg}_{0.60}\text{Fe}^{2+}_{0.40})\text{Si}_2\text{O}_6$	$\text{Fe}^{3+}_{0.15-0.20}\text{Al}_{0-0.03}\text{Ti}_{0.03-0.04}\text{V}_{0-0.005}\text{Mn}_{0.01}\text{Cr}_{0-0.004}$ $(\text{Si}_{1.74-1.81}\text{Al}_{0.19-0.23}\text{Fe}^{3+}_{0-0.02})_2\text{O}_6$
	$b = 8.9198$	$b = 8.899(5)$		
	$c = 5.2516$	$c = 5.252(3)$		
	$\beta = 105.86$	$\beta = 105.68(2)$		
Plagioclase	$a = 8.1736$ [43]	$a = 8.174(2)$	$\text{Na}_{1.9}\text{Ca}_{2.0}\text{Al}_6\text{Si}_{12}\text{O}_{32}$	$\text{Na}_{0.47-3.26}\text{Ca}_{0.52-3.59}\text{K}_{0-0.11}$ $\text{Fe}^{3+}_{0-0.2}\text{Al}_{4.57-7.32}\text{Si}_{8.46-11.54}\text{O}_{32}$
	$b = 12.8736$	$b = 12.880(3)$		
	$c = 7.1022$	$c = 7.112(2)$		
	$\alpha = 93.462$	$\alpha = 93.345(1)$		
	$\beta = 116.054$	$\beta = 116.30(5)$		
	$\gamma = 90.475$	$\gamma = 90.29(1)$		

The Rietveld refinement plots (Figures 3, 6, 9, 12, 15 and 18) show the observed and calculated patterns for the studied samples. All of the refinements are acceptable, as can be judged by the standard indices of agreement and by the visual fits of the observed and calculated diffraction profiles, considering the complexity of the pattern and the large number of reflections.

Each sample studied presents unique difficulties, as a result of its particular assemblages of minerals but the results show that the Rietveld XRPD method can be confidently applied to the wide range of rock types and phases under consideration here.

## 6. Conclusions

In the present study, we have shown that accurate mineral quantification may be obtained by the Rietveld XRPD method from inhomogeneous fine-zoned skarn rocks. The method is equally applicable to fine-grained and coarse-grained rocks, and is useful in distinguishing between the components in solid solutions phases.

The samples studied contain minerals with highly variable chemical compositions and involve up to eight major phases, causing significant overlap of peaks in the XRPD patterns. We demonstrate that the Rietveld XRPD method was able to refine these complex diffraction patterns. All of the refinements are acceptable, as can be judged by the standard indices of agreement and by the visual fit of the observed and calculated diffraction profiles.

Summarizing the discussed quantitative approach, we may claim that the considered technique is a serious tool for accurate and time saving quantitative determination of mineral contents in complex geological materials that may give important mineralogical information leading to additional genetic conclusions.

**Author Contributions:** Collection of the samples and optical studies, Y.T.; EPMA and SEM analyses, Y.T. and M.T.; Rietveld refinement procedures, Y.T., O.P., and T.K.; writing—original draft preparation, Y.T. and O.P.; writing—review and editing, Y.T., O.P., T.K. and M.T.; visualization, Y.T., O.P., T.K., and M.T.; All authors have read and agreed to the published version of the manuscript.

**Funding:** This research received no external funding.

**Acknowledgments:** The authors of this paper are thankful to the reviewers for their constructive comments and suggestions, which helped us to improve considerably the manuscript.

**Conflicts of Interest:** The authors declare no conflict of interest.

## Appendix A

**Table A1.** Representative EPMA analyses and structural formulae of garnets from skarn rocks in the Zvezdel–Pcheloyad ore deposit (Fe<sup>2+</sup> and Fe<sup>3+</sup> according to the charge balance).

Skarn Type	Grt Skarn						Cpx-Grt Skarn					Pl-Cpx-Wo-Grt		
No. of analyses	45-4-1	56	Gr-2-1	62	63	10	30	40	41	55-6-5	75	99	66	68
<i>Oxides (wt%)</i>														
SiO <sub>2</sub>	37.72	39.20	36.47	39.22	36.51	39.80	38.80	39.64	36.16	37.49	36.41	37.16	36.57	37.20
TiO <sub>2</sub>	0.00	0.11	0.87	0.00	1.14	0.03	0.00	0.00	0.81	0.00	0.82	1.03	1.06	0.20
Al <sub>2</sub> O <sub>3</sub>	9.25	20.09	8.64	18.62	10.98	17.49	20.01	20.66	10.72	8.41	11.52	11.99	11.32	7.35
Fe <sub>2</sub> O <sub>3</sub>	16.91	3.84	19.43	4.61	15.75	6.18	2.95	2.11	16.35	18.34	14.88	14.47	15.20	21.61
MnO	0.00	0.00	0.16	0.00	0.00	0.00	0.00	0.08	0.09	0.00	0.00	0.00	0.00	0.00
MgO	0.12	0.00	0.17	0.85	0.70	0.70	0.41	0.77	0.61	0.00	0.65	0.76	0.75	0.51
CaO	36.23	36.11	34.23	36.42	34.46	35.49	36.87	37.17	33.82	36.63	34.28	34.18	34.29	33.82
Total	100.23	99.35	99.97	99.72	99.54	99.69	99.04	100.43	98.56	100.87	98.56	99.59	99.19	100.69
<i>Structural formulae (a.p.f.u.) based on 12 oxygen atoms</i>														
Si	3.008	3.000	2.948	2.991	2.917	3.057	2.965	2.975	2.924	2.986	2.928	2.952	2.926	2.998
Al <sup>IV</sup>	0.000	0.000	0.052	0.009	0.083	0.000	0.035	0.025	0.076	0.014	0.072	0.048	0.074	0.002
Al <sup>VI</sup>	0.869	1.811	0.770	1.663	0.951	1.582	1.765	1.801	0.945	0.775	1.019	1.074	0.992	0.696
Fe <sup>3+</sup>	1.015	0.170	1.174	0.265	0.947	0.295	0.170	0.119	0.995	1.099	0.900	0.847	0.915	1.280
Ti	0.000	0.006	0.053	0.000	0.069	0.002	0.000	0.000	0.049	0.000	0.050	0.062	0.064	0.012
Fe <sup>2+</sup>	0.000	0.012	0.007	0.000	0.000	0.063	0.000	0.000	0.000	0.000	0.000	0.017	0.000	0.012
Fe <sup>2+</sup>	0.000	0.039	0.000	0.000	0.000	0.000	0.000	0.000	0.000	0.000	0.000	0.001	0.000	0.019
Mg	0.014	0.000	0.020	0.097	0.083	0.080	0.047	0.086	0.074	0.000	0.078	0.090	0.089	0.061
Mn	0.000	0.000	0.011	0.000	0.000	0.000	0.000	0.005	0.006	0.000	0.000	0.000	0.000	0.000
Ca	3.095	2.961	2.964	2.976	2.950	2.921	3.018	2.989	2.931	3.126	2.953	2.909	2.939	2.920
Adr	53.87	8.50	58.58	13.74	48.14	15.19	8.79	6.20	50.03	58.64	45.71	42.35	46.42	64.00
Grs	45.38	88.64	36.88	81.22	44.13	77.34	88.79	89.06	43.49	41.36	47.79	49.15	45.81	30.80
Prp	0.74	0.00	1.00	5.03	4.22	4.12	2.43	4.48	3.72	0.00	3.96	4.50	4.52	3.05
Sps	0.00	0.00	0.55	0.00	0.00	0.00	0.00	0.26	0.30	0.00	0.00	0.00	0.00	0.00
Schor + Morm	0.00	0.90	2.99	0.00	3.51	3.35	0.00	0.00	2.46	0.00	2.54	3.95	3.25	1.20
Alm	0.00	1.95	0.00	0.00	0.00	0.00	0.00	0.00	0.00	0.00	0.00	0.05	0.00	0.95

Notes: Adr, andradite; Grs, grossular; Prp, pyrope; Sps, spessartine; Uv, uvarovite; Schor+Morm, schorlomite+morimotoite; Gld, goldmanite; Alm, almandine.

**Table A2.** Representative EPMA analyses and structural formulae of subsilicic aluminian ferrian diopside (“fassaite”) from skarn rocks in the Zvezdel–Pcheloyad ore deposit (Fe<sup>2+</sup> and Fe<sup>3+</sup> according to the charge balance).

Skarn Type	Cpx-Grt Skarn								Pl-Cpx-Wo-Grt						
No. of anal.	P-9-4	P-4-1	Px-4-6	P-22	P-25	P-26	P-26a	P-26b	P-78	P-79	P-86	P-87	P-90	P-91	P-92
<i>Oxides (wt%)</i>															
SiO <sub>2</sub>	34.00	33.54	34.79	39.10	39.07	38.86	38.92	39.00	35.95	36.63	38.91	34.16	36.67	37.37	36.10
TiO <sub>2</sub>	2.26	2.70	2.47	1.28	0.57	1.24	0.63	0.63	1.00	0.92	0.69	1.14	0.72	0.77	0.97
Al <sub>2</sub> O <sub>3</sub>	16.86	17.43	17.72	16.25	15.91	16.54	16.53	16.61	17.69	17.75	15.34	17.64	16.85	16.43	16.88
FeO	16.40	0.00	0.00	11.50	9.67	10.51	10.81	10.60	13.70	13.95	11.59	16.21	13.69	12.67	13.93
Fe <sub>2</sub> O <sub>3</sub>	0.00	17.67	17.32	0.00	0.00	0.00	0.00	0.00	0.00	0.00	0.00	0.00	0.00	0.00	0.00
Cr <sub>2</sub> O <sub>3</sub>	0.00	0.00	0.08	0.00	0.00	0.00	0.00	0.00	0.00	0.00	0.00	0.00	0.00	0.00	0.00
MnO	0.00	0.00	0.18	0.00	0.09	0.22	0.08	0.08	0.00	0.00	0.08	0.00	0.00	0.00	0.00
MgO	4.40	4.35	4.92	7.76	8.37	8.15	8.19	8.17	5.88	5.96	7.61	5.02	5.90	6.56	5.90
CaO	25.01	23.92	24.24	25.40	25.18	25.38	25.26	25.26	24.37	25.12	25.30	24.87	24.75	25.17	24.99
Total	98.93	99.61	101.7	101.3	98.86	100.9	100.4	100.4	98.59	100.3	99.52	99.04	98.58	98.97	98.77
<i>Structural formulae (a.p.f.u.) based on 6 oxygen atoms</i>															
Si	1.325	1.322	1.337	1.454	1.476	1.445	1.452	1.455	1.384	1.386	1.472	1.320	1.413	1.428	1.389
Al <sup>IV</sup>	0.675	0.678	0.663	0.546	0.524	0.555	0.548	0.545	0.616	0.614	0.528	0.680	0.587	0.572	0.611
Al <sup>VI</sup>	0.099	0.131	0.140	0.165	0.184	0.169	0.178	0.185	0.187	0.177	0.156	0.124	0.177	0.168	0.155
Ti	0.066	0.080	0.071	0.036	0.016	0.035	0.018	0.018	0.029	0.026	0.020	0.033	0.021	0.022	0.028
Fe <sup>3+</sup>	0.441	0.383	0.374	0.308	0.305	0.315	0.333	0.322	0.368	0.382	0.330	0.487	0.366	0.357	0.398
Fe <sup>2+</sup>	0.094	0.140	0.127	0.050	0.001	0.012	0.004	0.008	0.073	0.060	0.036	0.037	0.075	0.048	0.051
Cr	0.000	0.000	0.002	0.000	0.000	0.000	0.000	0.000	0.000	0.000	0.000	0.000	0.000	0.000	0.000
Mg	0.256	0.256	0.282	0.430	0.472	0.452	0.455	0.454	0.338	0.336	0.429	0.289	0.339	0.374	0.339
Mn	0.000	0.000	0.006	0.000	0.003	0.007	0.003	0.003	0.000	0.000	0.003	0.000	0.000	0.000	0.000
Ca	1.044	1.010	0.998	1.012	1.019	1.011	1.009	1.010	1.006	1.019	1.026	1.030	1.022	1.031	1.031
Di+Hd	29.71	31.92	34.53	44.89	46.89	44.04	44.80	45.15	38.39	37.72	46.00	30.21	40.18	41.28	37.28
Ess	46.12	38.69	37.33	31.14	31.09	31.82	33.60	32.53	36.98	38.94	33.88	50.21	37.42	36.84	40.99
CaTs	10.36	13.23	13.97	16.68	18.76	17.07	17.96	18.69	18.79	18.04	16.02	12.78	18.10	17.34	15.96
S4(Mg)	13.81	16.16	14.17	7.28	3.26	7.07	3.63	3.64	5.83	5.30	4.11	6.80	4.29	4.54	5.77

Notes: Di, diopside; Hd, hedenbergite; Ess, esseneite; CaTs, Ca-Tschermak; S4 (Mg), component (CaMg<sub>0.5</sub>Ti<sub>4+0.5</sub>AlSiO<sub>6</sub>).

**Table A3.** Representative EPMA analyses and structural formulae of clinopyroxenes of the diopside–hedenbergite series from skarn rocks in the Zvezdel–Pcheloyad ore deposit (Fe<sup>2+</sup> and Fe<sup>3+</sup> according to the charge balance).

Skarn Type	Pl-Cpx-Wo-Ep Skarn						Pl-Cpx-Wo-Grt Skarn			Pl-Cpx-Wo Skarn			Pl-Cpx Skarn			
No. of anal.	P-15	P-17	P-18	P-19	P-20	P-21	13-11	P-104	P-94	11	12	12L	21	27	28	29
<i>Oxides (wt%)</i>																
SiO <sub>2</sub>	49.30	50.05	50.44	49.04	47.63	49.00	56.21	49.29	49.21	52.09	51.25	51.22	45.15	44.54	45.85	47.61
TiO <sub>2</sub>	0.40	0.37	0.38	0.55	0.70	0.58	0.00	0.24	0.18	0.00	0.00	0.00	1.38	1.51	1.02	0.89
Al <sub>2</sub> O <sub>3</sub>	3.73	3.39	2.68	3.45	3.65	4.25	0.65	3.09	2.90	0.83	0.95	0.95	4.98	5.06	5.65	4.44
FeO	10.72	10.82	9.64	11.12	15.54	10.75	1.08	11.66	8.11	7.99	8.38	8.39	16.37	16.87	11.88	11.39
Cr <sub>2</sub> O <sub>3</sub>	0.00	0.00	0.00	0.00	0.00	0.00	0.00	0.00	0.00	0.17	0.00	0.00	0.00	0.14	0.00	0.00
MnO	0.00	0.00	0.00	0.00	0.00	0.00	0.00	0.23	0.16	0.38	0.38	0.38	0.36	0.32	0.22	0.18
V <sub>3</sub> O <sub>4</sub>	0.00	0.00	0.00	0.00	0.00	0.00	0.00	0.00	0.00	0.00	0.00	0.00	0.13	0.17	0.00	0.11
MgO	10.11	10.78	11.91	10.24	7.69	10.00	16.73	10.23	12.47	12.77	12.31	12.3	7.51	7.26	9.67	10.54
CaO	25.32	25.41	25.13	24.77	23.87	24.80	24.06	24.15	25.28	24.68	24.54	24.54	22.89	22.71	23.49	23.9
Na <sub>2</sub> O	0.00	0.00	0.00	0.00	0.00	0.00	0.00	0.00	0.37	0.21	0.19	0.19	0.51	0.44	0.28	0.32
Total	99.58	100.82	100.18	99.17	99.08	99.38	98.73	98.89	98.68	99.12	98.00	98.9	99.28	99.02	98.06	99.38
<i>Structural formulae (a.p.f.u.) based on 6 oxygen atoms</i>																
Si	1.875	1.877	1.892	1.875	1.859	1.868	2.070	1.892	1.856	1.964	1.958	1.957	1.756	1.742	1.772	1.81
Al <sup>IV</sup>	0.125	0.123	0.108	0.125	0.141	0.132	0.000	0.108	0.129	0.036	0.042	0.043	0.228	0.233	0.228	0.19
Fe <sup>3+IV</sup>	0.000	0.000	0.000	0.000	0.000	0.000	0.000	0.000	0.015	0.000	0.000	0.000	0.016	0.025	0.000	0.000
Al <sup>VI</sup>	0.042	0.027	0.011	0.030	0.027	0.059	0.028	0.032	0.000	0.001	0.000	0.000	0.000	0.000	0.029	0.009
Ti	0.011	0.010	0.011	0.016	0.021	0.017	0.000	0.007	0.005	0.000	0.000	0.000	0.04	0.044	0.03	0.025
Fe <sup>3+</sup>	0.059	0.075	0.075	0.063	0.073	0.039	0.000	0.061	0.161	0.045	0.056	0.055	0.201	0.197	0.161	0.153
Fe <sup>2+</sup>	0.282	0.264	0.227	0.293	0.435	0.304	0.033	0.313	0.080	0.207	0.212	0.212	0.315	0.329	0.223	0.209
Cr	0.000	0.000	0.000	0.000	0.000	0.000	0.000	0.000	0.000	0.005	0.000	0.000	0.000	0.004	0.000	0.000
Mg	0.573	0.603	0.666	0.584	0.447	0.568	0.919	0.586	0.701	0.718	0.701	0.701	0.435	0.423	0.557	0.597
V	0.000	0.000	0.000	0.000	0.000	0.000	0.000	0.000	0.000	0.000	0.000	0.000	0.004	0.005	0.000	0.003
Mn	0.000	0.000	0.000	0.000	0.000	0.000	0.000	0.007	0.005	0.012	0.012	0.012	0.012	0.011	0.007	0.006
Ca	1.032	1.021	1.010	1.015	0.998	1.013	0.950	0.993	1.021	0.997	1.004	1.005	0.954	0.952	0.972	0.974
Na	0.000	0.000	0.000	0.000	0.000	0.000	0.000	0.000	0.027	0.015	0.014	0.014	0.038	0.033	0.021	0.024
Jd	0.00	0.00	0.00	0.00	0.00	0.00	0.00	0.00	0.00	0.04	0.03	0.01	0.00	0.00	1.18	0.49
Aeg	0.00	0.00	0.00	0.00	0.00	0.00	0.00	0.00	1.48	0.75	0.70	0.72	2.21	1.92	0.00	0.82
Ess	3.13	3.98	3.96	3.31	3.87	2.06	0.00	3.23	7.31	1.86	2.18	2.15	9.35	9.69	9.05	7.68
CTTs	0.61	0.55	0.56	0.84	1.09	0.88	0.00	0.37	0.28	0.00	0.00	0.00	2.32	2.56	1.67	1.41
CaTs	2.24	1.41	0.56	1.60	1.42	3.13	0.00	1.70	0.00	0.00	0.00	0.00	0.00	0.00	0.44	0.00
Wo	48.70	48.14	47.99	47.90	46.71	47.66	49.94	47.21	48.26	49.63	49.82	49.86	43.07	42.52	43.66	44.89
En	30.38	31.92	35.00	30.86	23.80	30.15	48.31	30.94	38.33	37.06	36.29	36.27	24.99	24.36	31.40	33.13
Fs	14.94	14.00	11.94	15.49	23.11	16.12	1.75	16.56	4.35	10.66	10.98	10.99	18.07	18.96	12.59	11.58

Notes: Jd, jadeite; Aeg, aegirine; Ess, esseneite; CTTs, component (CaTiAlAlO<sub>6</sub>); CaTs, Ca-Tschermak; Wo, wollastonite; En, enstatite; Fs, ferrosilite.

**Table A4.** Representative EPMA analyses and structural formulae of wollastonite from skarn rocks in the Zvezdel–Pcheloyad ore deposit.

Skarn Type	Pl-Cpx-Wo-Grt Skarn								Pl-Cpx-Wo Skarn		Pl-Cpx-Wo-Ep Skarn					
	No. of anal.	103	67	70	71	72	73	77	81	18	19	1	10	31	6	W-2-1
<i>Oxides (wt%)</i>																
SiO <sub>2</sub>	50.26	50.89	52.07	51.62	51.00	51.37	51.27	50.81	50.74	50.68	53.58	53.43	53.59	51.66	51.56	51.91
TiO <sub>2</sub>	0.00	0.00	0.00	0.00	0.00	0.00	0.00	0.00	0.00	0.00	0.00	0.00	0.00	0.00	0.00	0.19
Al <sub>2</sub> O <sub>3</sub>	0.89	0.95	1.07	1.12	1.07	1.08	0.96	1.01	0.00	0.36	0.00	0.00	0.00	0.00	0.22	0.14
Cr <sub>2</sub> O <sub>3</sub>	0.00	0.00	0.00	0.00	0.00	0.00	0.00	0.00	0.16	0.00	0.00	0.00	0.00	0.00	0.00	0.18
FeO	0.71	0.48	0.60	0.73	0.54	0.48	0.83	0.48	0.50	0.70	0.85	0.51	0.93	0.70	0.97	1.51
MnO	0.00	0.00	0.00	0.00	0.00	0.00	0.00	0.00	0.15	0.00	0.00	0.00	0.00	0.00	0.00	0.00
MgO	0.47	0.00	0.30	0.39	0.00	0.00	0.48	0.52	0.00	0.28	0.00	0.56	0.34	0.00	0.40	0.56
CaO	46.83	46.87	47.27	46.97	46.29	47.45	46.47	47.04	47.17	46.92	45.29	44.34	45.12	48.27	46.43	45.81
Total	99.16	99.19	101.31	100.83	98.90	100.38	100.01	99.86	98.72	98.94	99.72	98.84	99.98	100.63	99.58	100.30
<i>Structural formulae (a.p.f.u.) based on 6 oxygen atoms</i>																
Si	1.964	1.982	1.982	1.976	1.988	1.977	1.979	1.967	1.993	1.984	2.056	2.060	2.051	1.992	2.000	2.000
Al	0.041	0.044	0.048	0.050	0.049	0.049	0.044	0.046	0.000	0.017	0.000	0.000	0.000	0.000	0.010	0.006
Ti	0.000	0.000	0.000	0.000	0.000	0.000	0.000	0.000	0.000	0.000	0.000	0.000	0.000	0.000	0.000	0.006
Fe <sup>2+</sup>	0.023	0.016	0.019	0.023	0.018	0.015	0.027	0.016	0.016	0.023	0.027	0.016	0.030	0.023	0.031	0.049
Cr	0.000	0.000	0.000	0.000	0.000	0.000	0.000	0.000	0.005	0.000	0.000	0.000	0.000	0.000	0.000	0.005
Mn	0.000	0.000	0.000	0.000	0.000	0.000	0.000	0.000	0.005	0.000	0.000	0.000	0.000	0.000	0.000	0.000
Mg	0.027	0.000	0.017	0.022	0.000	0.000	0.028	0.030	0.000	0.016	0.000	0.032	0.019	0.000	0.023	0.032
Ca	1.960	1.956	1.928	1.926	1.933	1.957	1.922	1.951	1.985	1.968	1.862	1.832	1.850	1.994	1.930	1.891

**Table A5.** Representative EPMA analyses and structural formulae of plagioclase from skarn rocks in the Zvezdel–Pcheloyad ore deposit.

Skarn Type	Pl-Cpx-Wo Skarn					Pl-Cpx Skarn				Pl-Cpx-Wo-Grt Skarn				Pl-Cpx-Wo-Ep Skarn					
	No. of anal.	01	14	20	18–13	23	24	25	31	33	Ab1	Ab1a	107	108	2 10	27 10	3 10	4 10	5 10
<i>Oxides (wt%)</i>																			
SiO <sub>2</sub>	67.65	67.26	41.67	61.58	44.44	54.64	64.17	51.88	63.85	67.41	67.42	67.80	68.47	44.98	64.53	51.87	66.29	61.70	51.70
Al <sub>2</sub> O <sub>3</sub>	19.36	19.19	29.82	22.24	32.68	26.17	21.22	27.77	21.65	19.04	19.05	19.40	19.43	33.69	21.03	30.27	20.71	30.19	30.19
Fe <sub>2</sub> O <sub>3</sub>	0.00	0.00	0.29	0.00	1.25	1.19	0.00	1.42	0.00	0.20	0.20	0.00	0.00	1.10	0.00	0.00	0.00	0.00	0.00
MgO	0.00	0.00	0.00	1.17	0.00	0.00	0.00	0.00	0.00	0.00	0.00	0.00	0.00	0.00	0.00	0.00	0.00	0.00	0.00
CaO	0.43	0.37	10.95	0.29	17.61	9.63	2.69	11.65	2.97	0.35	0.34	0.52	0.00	18.86	11.16	15.29	2.67	14.17	14.17
Na <sub>2</sub> O	11.43	10.74	2.39	11.18	1.27	5.60	9.35	4.43	9.57	11.46	11.48	11.47	12.08	0.35	1.70	2.14	9.47	2.82	2.82
K <sub>2</sub> O	0.08	0.00	0.00	1.32	0.00	0.49	0.10	0.26	0.08	0.19	0.17	0.00	0.00	0.00	0.50	0.00	0.00	0.00	0.00
Total	98.95	97.56	85.12	0.90	97.25	97.72	97.53	97.41	98.12	98.65	98.66	99.19	99.98	98.98	98.92	99.57	99.14	98.88	98.88
<i>Structural formulae (a.p.f.u.) based on 32 oxygen atoms</i>																			
Si	11.952	12.007	8.863	11.087	8.456	10.109	11.544	9.685	11.447	11.963	11.962	11.948	11.972	8.402	11.461	9.446	11.704	9.470	9.470
Al	4.028	4.034	7.470	4.715	7.323	5.702	4.496	6.105	4.571	3.979	3.981	4.026	4.001	7.411	4.399	6.492	4.306	6.512	6.512
Fe <sup>3+</sup>	0.000	0.000	0.046	0.000	0.179	0.166	0.000	0.199	0.000	0.027	0.027	0.000	0.000	0.154	0.000	0.000	0.000	0.000	0.000
Mg	0.000	0.000	0.000	0.178	0.000	0.000	0.000	0.000	0.000	0.000	0.000	0.000	0.000	0.000	0.000	0.000	0.000	0.000	0.000
Ca	0.081	0.071	2.495	0.078	3.590	1.909	0.519	2.330	0.570	0.067	0.065	0.098	0.000	3.774	2.124	2.983	0.505	2.781	2.781
Na	3.916	3.717	0.986	2.157	0.469	2.009	3.262	1.604	3.327	3.943	3.950	3.919	4.096	0.127	0.585	0.756	3.242	1.002	1.002
K	0.018	0.000	0.000	0.461	0.000	0.116	0.023	0.062	0.018	0.043	0.038	0.000	0.000	0.000	0.113	0.000	0.000	0.000	0.000
Ab	97.50	98.10	28.30	16.30	11.60	49.80	85.80	40.10	85.00	97.30	97.50	97.60	100.0	3.30	20.70	20.20	86.50	26.50	26.50
An	2.00	1.90	71.70	76.40	88.40	47.30	13.60	58.30	14.60	1.70	1.60	2.40	0.00	96.70	75.30	79.80	13.50	73.50	73.50
Or	0.40	0.00	0.00	7.30	0.00	2.90	0.60	1.60	0.50	1.10	0.90	0.00	0.00	0.00	4.00	0.00	0.00	0.00	0.00

Notes: Ab, albite; An, anorthite; Or, orthoclase.

**Table A6.** Representative EPMA analyses and structural formulae of epidote from skarn rocks in the Zvezdel–Pcheloyad ore deposit.

Skarn Type	Pl-Cpx-Wo-Ep Skarn											
No. of anal.	E25-7	E25-6	E27-6	Ep-6-8	E8-2-2	Ep-2-2	E19-1	E29-3	E19-2	E19-5	E29-6	E19-9
<i>Oxides (wt%)</i>												
SiO <sub>2</sub>	38.63	38.59	36.73	37.76	37.36	37.59	37.82	37.24	37.42	36.93	37.22	37.15
Al <sub>2</sub> O <sub>3</sub>	25.64	25.62	20.41	22.35	20.53	21.30	23.45	21.28	22.12	23.71	22.96	24.08
Fe <sub>2</sub> O <sub>3</sub>	8.20	9.11	14.63	13.61	14.38	15.01	13.83	14.25	12.98	11.38	12.42	10.53
CaO	24.11	24.09	24.04	22.98	23.74	23.10	23.31	23.11	23.72	23.29	23.19	23.18
Total	96.58	97.41	95.81	96.70	96.01	97.00	98.41	95.88	96.24	95.31	95.79	94.94
<i>Structural formulae (a.p.f.u.) based on 12.5 oxygen atoms</i>												
Si	3.062	3.042	3.024	3.045	3.058	3.041	2.998	3.008	3.005	2.978	2.993	2.998
Al	2.394	2.378	1.979	2.122	1.979	2.029	2.191	2.026	2.094	2.253	2.176	2.290
Fe <sup>3+</sup>	0.489	0.540	0.906	0.825	0.885	0.913	0.825	0.963	0.872	0.767	0.835	0.711
Ca	2.048	2.035	2.121	1.985	2.082	2.002	1.980	2.000	2.041	2.012	1.998	2.004
X <sub>Fe</sub>	0.17	0.19	0.31	0.28	0.31	0.31	0.27	0.32	0.29	0.25	0.28	0.24

$$X_{\text{Fe}} = \text{Fe}^{3+}/(\text{Fe}^{3+} + \text{Al}).$$

**Table A7.** Representative EPMA analyses and structural formulae of prehnite from skarn rocks in the Zvezdel–Pcheloyad ore deposit.

Skarn Type	Pl-Cpx-Wo-Grt Skarn				Pl-Cpx-Wo+Ep Skarn			Cpx-Grt Skarn	Pl-Cpx-Wo Skarn		
No. of anal.	101	102	74	83	P26-6	P-7-2-9	69	11	3	4	9
<i>Oxides (wt%)</i>											
SiO <sub>2</sub>	44.58	45.64	43.25	43.78	43.42	42.83	43.67	43.87	43.54	44.04	43.39
TiO <sub>2</sub>	0.00	0.00	0.00	0.00	0.00	0.00	0.00	0.00	0.16	0.21	0.00
Al <sub>2</sub> O <sub>3</sub>	24.78	24.90	23.92	22.52	21.74	20.46	19.41	22.82	22.06	23.10	23.85
Fe <sub>2</sub> O <sub>3</sub>	0.95	0.00	0.62	2.08	2.99	4.28	7.15	1.89	3.38	1.86	0.23
MgO	0.00	0.00	0.00	0.33	0.00	0.00	0.00	0.29	0.00	0.00	0.00
CaO	26.77	27.25	27.32	27.28	27.72	27.68	25.77	25.94	26.53	26.57	26.53
Total	97.08	97.79	95.11	95.99	95.87	95.25	96.00	94.81	95.67	95.78	94.00
<i>Structural formulae (a.p.f.u.) based on 11 oxygen atoms</i>											
Si	3.013	3.052	2.997	3.020	3.016	3.014	3.053	3.046	3.020	3.031	3.028
Al	1.973	1.961	1.952	1.830	1.778	1.695	1.598	1.866	1.802	1.873	1.960
Fe <sup>3+</sup>	0.048	0.000	0.032	0.108	0.156	0.226	0.376	0.099	0.176	0.096	0.012
Ti	0.000	0.000	0.000	0.000	0.000	0.000	0.000	0.000	0.017	0.022	0.000
Mg	0.000	0.000	0.000	0.034	0.000	0.000	0.000	0.030	0.000	0.000	0.000
Ca	1.939	1.952	2.028	2.016	2.063	2.087	1.930	1.929	1.972	1.960	1.983

## References

1. Rietveld, H.M. Line profiles of neutron powder-diffraction peaks for structure refinement. *Acta Crystallogr.* **1967**, *22*, 151–152. [[CrossRef](#)]
2. Rietveld, H.M. A profile refinement method for nuclear and magnetic structures. *J. Appl. Cryst.* **1969**, *2*, 65–71. [[CrossRef](#)]
3. Young, R.A.; Mackie, P.E.; Von Dreele, R.B. Application of the pattern-fitting structure-refinement method to X-ray powder diffractometer patterns. *J. Appl. Cryst.* **1977**, *10*, 262–269. [[CrossRef](#)]
4. Hill, R.J. X-ray powder diffraction profile refinement of synthetic hercynite. *Am. Mineral.* **1984**, *69*, 937–942.
5. Cox, D.E.; Hastings, J.B.; Thomlinson, W.; Prewitt, C.T. Application of synchrotron radiation to high resolution powder diffraction and Rietveld refinement. *Nucl. Instrum. Methods Phys. Res.* **1983**, *208*, 573–578. [[CrossRef](#)]
6. Bish, D.L. Rietveld refinement of the kaolinite structure at 1.5 K. *Clays Clay Miner.* **1993**, *41*, 738–744. [[CrossRef](#)]
7. Albinati, A.; Willis, B.T.M. The Rietveld method in X-ray and neutron powder diffraction. *J. Appl. Crystallogr.* **1982**, *15*, 361–374. [[CrossRef](#)]
8. Hill, R.J. Calculated X-ray powder diffraction data for phases encountered in lead/acid battery plates. *J. Power Sources* **1983**, *9*, 55–71. [[CrossRef](#)]
9. Hill, R.J.; Madsen, I.C. Data collection strategies for constant wavelength Rietveld analysis. *Powder Diffr.* **1987**, *2*, 146–162. [[CrossRef](#)]
10. Hill, R.J.; Howard, C.J. Quantitative phase analysis from neutron powder diffraction data using the Rietveld method. *J. Appl. Cryst.* **1987**, *20*, 467–474. [[CrossRef](#)]
11. Bish, D.L.; Howard, S.A. Quantitative phase analysis using the Rietveld method. *J. Appl. Crystallogr.* **1988**, *21*, 86–91. [[CrossRef](#)]
12. Post, J.E.; Bish, D.L. Rietveld Refinement of Crystal Structures Using Powder X-Ray Diffraction Data. In *Modern Powder Diffraction; Reviews in Mineralogy*; Bish, D.L., Post, J.E., Eds.; Mineralogical Society of America: Washington, DC, USA, 1989; Volume 20, pp. 277–308.
13. Snyder, R.L.; Bish, D.L. Quantitative Analysis. In *Modern Powder Diffraction; Reviews in Mineralogy*; Bish, D.L., Post, J.E., Eds.; Mineralogical Society of America: Washington, DC, USA, 1989; Volume 20, pp. 277–308.
14. Hill, R.J. Expanded use of the Rietveld method in studies of phase abundance in multiphase mixtures. *Powder Diffr.* **1991**, *6*, 74–77. [[CrossRef](#)]
15. Young, R.A. Introduction to the Rietveld Method. In *The Rietveld Method*; International Union of Crystallography, Monographs in Crystallography; Young, R.A., Ed.; Oxford University Press: New York NY, USA, 1993; pp. 1–38.
16. Bish, D.L.; Post, J.E. Quantitative mineralogical analysis using the Rietveld full-pattern fitting method. *Am. Mineral.* **1993**, *78*, 932–940.
17. McCusker, L.B.; Von Dreele, R.B.; Cox, D.E.; Louër, D.; Scardi, P. Rietveld refinement guidelines. *J. Appl. Cryst.* **1999**, *32*, 36–50. [[CrossRef](#)]
18. Hill, R.J.; Tsambourakis, G.; Madsen, I.C. Improved petrological modal analyses from X-ray powder diffraction data by use of the Rietveld method I. Selected igneous, volcanic, and metamorphic rocks. *J. Pet.* **1993**, *34*, 867–900. [[CrossRef](#)]
19. Mumme, W.G.; Tsambourakis, G.; Madsen, I.C.; Hill, J.R. Improved petrological modal analyses from X-ray powder diffraction data by use of the Rietveld method. Part II. Selected sedimentary rocks. *J. Sediment. Res.* **1996**, *66*, 132–138.
20. Mumme, W.G.; Tsambourakis, G.; Cranswick, L.M.D. Improved petrological modal analyses from X-ray and neutron powder diffraction data by use of the Rietveld method. Part 3. Selected massive sulphide ores. *J. Petrol.* **1996**, *170*, 231–255.
21. Taylor, J.C.; Matulis, C.E. A new method for Rietveld clay analysis. Part, I. Use of a universal measured standard profile for Rietveld quantification of montmorillonites. *Powder Diffr.* **1994**, *9*, 119–123. [[CrossRef](#)]
22. Raudsepp, M.; Pani, E.; Dipple, G.M. Measuring mineral abundance in skarn. I. The Rietveld method using X-ray powder-diffraction data. *Can. Miner.* **1999**, *37*, 1–15.
23. Monecke, T.; Köhler, S.; Kleeberg, R.; Herzig, P.; Gemmill, J.B. Quantitative phase-analysis by the Rietveld method using X-ray powder-diffraction data: Application to the study of alteration halos associated with volcanic-rock-hosted massive sulfide deposits. *Can. Mineral.* **2001**, *39*, 1617–1633. [[CrossRef](#)]

24. Webster, J.R.; Kight, R.P.; Winburn, R.S.; Cool, C.A. Heavy mineral analysis of sandstones by Rietveld analysis. *Adv. X-ray Anal.* **2003**, *46*, 198–203.
25. Gonzalez, R.M.; Edwards, T.E.; Lorbiecke, T.D.; Winburn, R.S.; Webster, J.R. Analysis of geologic materials using Rietveld quantitative X-ray diffraction. *Adv. X-Ray Anal.* **2003**, *46*, 204–209.
26. Oerter, E.J.; Brimhall, G.H., Jr.; Redmond, J.; Walker, B. A method for quantitative pyrite abundance in mine rock piles by powder X-ray diffraction and Rietveld refinement. *Appl. Geochem.* **2007**, *22*, 2907–2925. [[CrossRef](#)]
27. Ufer, K.; Stanjek, H.; Roth, G.; Dohrmann, R.; Kleeberg, R.; Kaufhold, S. Quantitative phase analysis of bentonites by the Rietveld method. *Clays Clay Miner.* **2008**, *56*, 272–282. [[CrossRef](#)]
28. Snellings, R.; Machiels, L.; Mertens, G.; Elsen, J. Rietveld refinement strategy for quantitative phase analysis of partially amorphous zeolitized tuffaceous rocks. *Geol. Belg.* **2010**, *13*, 183–196.
29. Hestnes, K.H.; Sørensen, B.E. Evaluation of quantitative X-ray diffraction for possible use in the quality control of granitic pegmatite in mineral production. *Min. Eng.* **2012**, *39*, 239–247. [[CrossRef](#)]
30. Gentili, S.; Comodi, P.; Bonadiman, C.; Coltorti, M. Mass balance vs Rietveld refinement to determine the modal composition of ultramafic rocks: The case study of mantle peridotites from Northern Victoria Land (*Antarctica*). *Tectonophysics* **2015**, *650*, 144–145. [[CrossRef](#)]
31. Santini, T.C. Application of the Rietveld refinement method for quantification of mineral concentrations in bauxite residues (*alumina refining tailings*). *Int. J. Miner. Process.* **2015**, *139*, 1–10. [[CrossRef](#)]
32. Santos, H.N.; Neumann, R.; Ávila, C.A. Mineral quantification with simultaneous refinement of Ca-Mg carbonates non-stoichiometry by X-ray diffraction, Rietveld method. *Minerals* **2017**, *7*, 164. [[CrossRef](#)]
33. Dietel, J.; Ufer, K.; Kaufhold, S.; Dohrmann, R. Crystal structure model development for soil clay minerals—II. Quantification and characterization of hydroxy-interlayered smectite (HIS) using the Rietveld refinement technique. *Geoderma* **2019**, *347*, 1–12. [[CrossRef](#)]
34. Nedialkov, R.; Mavroudchiev, B. Geochemical and mineralogical peculiarities of the Zvezdel pluton (East Rhodopes, Bulgaria). In Proceedings of the XV Congress of the Carpatho-Balkan Geological Association, Geol. Soc., Athens, Greece, 17–20 September 1995; pp. 561–565.
35. Tzvetanova, Y. Crystal-Chemical and Structural Characteristics of Minerals from Skarns in Zvezdel Pluton. Ph.D. Thesis, Institute of Mineralogy and Crystallography, Bulgarian Academy of Sciences, Sofia, Bulgaria, 2015.
36. Tzvetanova, Y.; Kadyiski, M.; Petrov, O. Parawollastonite (wollastonite-2M polytype) from the skarns in Zvezdel pluton, Eastern Rhodopes—A single crystal study. *Bulg. Chem. Commun.* **2012**, *44*, 131–136.
37. *Powder Diffraction File (PDF-2 Data Base 2001)*; International Centre for Diffraction Data (ICDD): Newtown Square, PA, USA, 2001.
38. Rodríguez-Carvajal, J.; Roisnel, T. *FullProf.98 and WinPLOTR New Windows 95/NT Applications for Diffraction*. Newsletter No 20. Commission for Powder Diffraction; International Union for Crystallography: Chester, UK, 1998.
39. Roisnel, T.; Rodríguez-Carvajal, J. WinPLOTR: A Windows tool for powder diffraction patterns analysis. *Mater. Sci. Forum* **2001**, *378*, 118–123. [[CrossRef](#)]
40. Rodríguez-Carvajal, J. Recent advances in magnetic structure determination by neutron powder diffraction. *Phys. B Condens. Matter.* **1993**, *192*, 55–69. [[CrossRef](#)]
41. *Topas V 4.2: General Profile and Structure Analysis Software for Powder Diffraction*; Bruker AXS: Karlsruhe, Germany, 2009.
42. Armbruster, T.; Bürgi, H.B.; Kunz, M.; Gnos, E.; Brönnimann, S.; Lienert, C. Variation of displacement parameters in structure refinements of low albite. *Am. Mineral.* **1990**, *75*, 135–140.
43. Wenk, H.R.; Joswig, W.; Tagai, T.; Korekawa, M.; Smith, B.K. The average structure of an 62–66 labradorite. *Am. Mineral.* **1980**, *65*, 81–95.
44. Lager, G.A.; Armbruster, T.; Rotella, F.J.; Rossman, G.R. OH substitution in garnets: X-ray and neutron diffraction, infrared and geometric-modeling studies. *Am. Mineral.* **1989**, *74*, 840–851.
45. Hazen, R.M.; Finger, L.W. Crystal structures and compressibilities of pyrope and grossular to 60 kbar. *Am. Mineral.* **1978**, *63*, 297–303.
46. Levien, L.; Prewitt, C.T. High-pressure structural study of diopside. *Am. Mineral.* **1981**, *66*, 315–323.
47. Cameron, M.; Sueno, S.; Prewitt, C.T.; Papike, J.J. High-temperature crystal chemistry of acmite, diopside, hedenbergite, jadeite, spodumene, and ureyite. *Am. Mineral.* **1973**, *58*, 594–618.

48. Cosca, M.A.; Peacor, D.R. Chemistry and structure of esseneite (CaFe<sup>3+</sup>AlSiO<sub>6</sub>), a new pyroxene produced by pyrometamorphism. *Am. Miner.* **1987**, *72*, 148–156.
49. Hesse, K.F. Refinement of the crystal structure of wollastonite-2M (*parawollastonite*). *Z. Kristallogr.* **1984**, *168*, 93–98. [[CrossRef](#)]
50. Dollase, W.A. Refinement of the crystal structures of epidote, allanite and hancockite. *Am. Mineral.* **1971**, *56*, 447–464.
51. Papike, J.J.; Zoltai, T. Ordering of tetrahedral aluminium in prehnite, Ca<sub>2</sub>(Al, Fe<sup>+3</sup>)[Si<sub>3</sub>AlO<sub>10</sub>](OH)<sub>2</sub>. *Am. Mineral.* **1967**, *52*, 974–984.
52. Effenberger, H.; Mereiter, K.; Zemmann, J. Crystal structure refinements of magnesite, calcite, rhodochrosite, siderite, smithsonite, and dolomite, with discussions of some aspects of the stereochemistry of calcite-type carbonates. *Z. Kristallogr.* **1981**, *156*, 233–243.
53. Levien, L.; Prewitt, C.T.; Weidner, D.J. Structure and elastic properties of quartz at pressure. *Am. Mineral.* **1980**, *65*, 920–930.
54. Zanazzi, P.F.; Comodi, P.; Nazzareni, S.; Andreozzi, G.B. Thermal behaviour of chlorite: An in situ single-crystal and powder diffraction study. *Eur. J. Mineral.* **2009**, *21*, 581–589. [[CrossRef](#)]
55. Hill, R.J.; Madsen, I.C. Rietveld analysis using para-focusing and Debye-Scherrer geometry data collected with a Bragg-Brentano diffractometer. *Z. Kristallogr.* **1991**, *196*, 73–92. [[CrossRef](#)]
56. Young, R.A.; Prince, E.; Sparks, R.A. Suggested guidelines for the publication of Rietveld analyses and pattern decomposition studies. *J. Appl. Cryst.* **1982**, *15*, 357–359. [[CrossRef](#)]



© 2020 by the authors. Licensee MDPI, Basel, Switzerland. This article is an open access article distributed under the terms and conditions of the Creative Commons Attribution (CC BY) license (<http://creativecommons.org/licenses/by/4.0/>).